# Accepted Manuscript

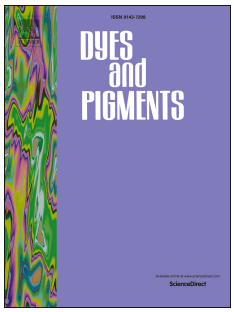


Violet-blue emitting 2-(*N*-alkylimino)pyrrolyl organoboranes: Synthesis, structure and luminescent properties

Paramasivam Krishnamoorthy, Bruno Ferreira, Clara S.B. Gomes, Diogo Vila-Viçosa, Ana Charas, Jorge Morgado, Maria José Calhorda, António L. Maçanita, Pedro T. Gomes

PII: S0143-7208(16)30846-4

DOI: 10.1016/j.dyepig.2016.11.017

Reference: DYPI 5586

To appear in: *Dyes and Pigments*

Received Date: 27 September 2016

Revised Date: 10 November 2016

Accepted Date: 14 November 2016

Please cite this article as: Krishnamoorthy P, Ferreira B, Gomes CSB, Vila-Viçosa D, Charas A, Morgado J, Calhorda MJ, Maçanita AL, Gomes PT, Violet-blue emitting 2-(*N*-alkylimino)pyrrolyl organoboranes: Synthesis, structure and luminescent properties, *Dyes and Pigments* (2016), doi: 10.1016/j.dyepig.2016.11.017.

**Graphical Abstract sentence:**

Violet-blue emitting 2-(*N*-Alkylimino)pyrrolyl organoboranes are synthesized, their structure and luminescent properties being described

**Graphical Abstract figure:**

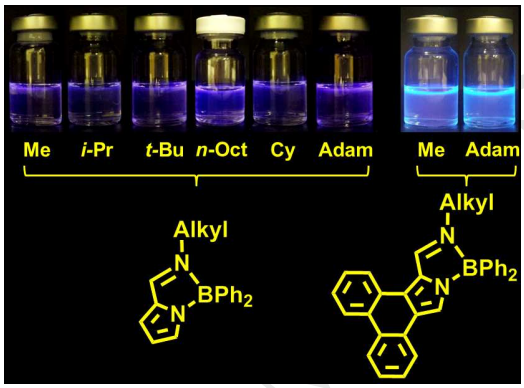

# Violet-Blue emitting 2-(*N*-Alkylimino)pyrrolyl Organoboranes: Synthesis, Structure and Luminescent Properties

Paramasivam Krishnamoorthy [a], Bruno Ferreira [a], Clara S.B. Gomes [a], Diogo Vila-Viçosa [d], Ana Charas [b], Jorge Morgado [b,c], Maria José Calhorda [d], António L. Maçanita [a], Pedro T. Gomes[a,*]

[a] Centro de Química Estrutural, Departamento de Engenharia Química, Instituto Superior Técnico, Universidade de Lisboa, Av. Rovisco Pais, 1049-001 Lisboa, Portugal.

[b] Instituto de Telecomunicações, Av. Rovisco Pais, 1049-001 Lisboa, Portugal.

[c] Department of Bioengineering, Instituto Superior Técnico, Universidade de Lisboa, Av. Rovisco Pais, 1049-001 Lisboa, Portugal.

[d] Centro de Química e Bioquímica, DQB, Faculdade de Ciências, Universidade de Lisboa, Campo Grande, Ed. C8, 1749-016 Lisboa, Portugal.

* Corresponding author: Pedro T. Gomes; E-mail: pedro.t.gomes@tecnico.ulisboa.pt

**Abstract**

The condensation reactions of 2-formylpyrrole (**1**) or 2-formylphenanthro[9,10-*c*]pyrrole (**2**) with various aliphatic amines afforded the corresponding 2-iminopyrrole ligand precursors **3**–**10**, which, upon stoichiometric reaction with $BPh_3$, led to the new mononuclear boron chelate compounds $Ph_2B[NC_4H_3C(H)=N\text{-}R]$ (R = Me **11**; *i*Pr **12**; *t*Bu **13**; *n*Oct **14**; Cy **15**; Adam **16**), and $Ph_2B(NC_{16}H_9C(H)=N\text{-}R)$ (R = Me **17**; Adam **13**), respectively. Boron complexes **11**–**16**, containing a simple 2-(*N*-alkylformimino)pyrrolyl ligand, are violet emitters and showed relatively modest fluorescence quantum efficiencies in solution (10% – 16%), whereas complexes **17** and **18**, bearing the π-extended 2-(*N*-alkylformimino)phenanthro[9,10-*c*]pyrrolyl ligand, are blue emitters presenting enhanced quantum efficiencies of 35% and 43%, respectively, in THF solution. DFT and TDDFT calculations were in good agreement with experimental results, showing that π systems (pyrrolyl and phenanthropyrrolyl in this case) have a strong influence on the observed optical properties by changing the nature of the low energy transitions. Non-doped single-layer light-emitting diodes (OLEDs) were fabricated with complexes **11**–**18**, deposited essentially by spin coating, those of complexes **17** and **18** revealing maximum luminances of 69 and 88 cd $m^{-2}$, respectively.

**Keywords**

Iminopyrrolyl ligands; Boron; Fluorescence; DFT; OLED

**Graphical Abstract**

Violet-blue emitting 2-(N-Alkylimino)pyrrolyl organoboranes are synthesized, their structure and luminescent properties being described.

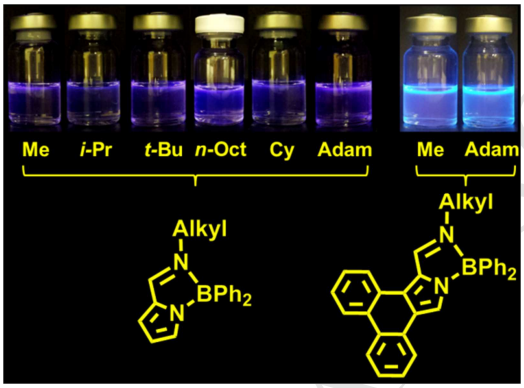

**Highlights**

- Several 2-(*N*-alkylimino)pyrrolyl diphenyl boron complexes were synthesized
- Fluorescence properties of these blue-violet emitting compounds were studied
- Non-radiative decays are much weaker than those of the *N*-2,6-$R_2$-arylimino analogues
- DFT and TDDFT calculations support the experimental results
- Simple OLED devices reveal maximum luminances of *ca.* 90 cd $m^{-2}$

## 1. Introduction

Organic Light Emitting Diode (OLED) based flat panel displays for cell phones, digital cameras, and TV sets are already commercially available. Despite this success, there is a strong claim for a next generation of flexible, highly luminous and economically improved red, green, blue and white OLEDs for displays and lighting applications, the two latter colors being highly requested. Because of these needs, research involving luminescent organic and organometallic complexes has received considerable attention [1].

Among them, the four-coordinate organoboron compounds are promising light emitting materials owing to their intense luminescence and high carrier mobility. Various types of tetracoordinate boron compounds containing different types of ligands, such as *N*,*O*-, *N*,*N*-, *N*,*C*-, *C*,*C*-, *C*,*O*-, and *O*,*O*-chelates, have been analyzed, their photophysical properties being strongly dependent upon the nature of the chelate ligand [2].

The 2-iminopyrrolyl ligands are an important class of anionic bidentate ($N,N^-$) chelates, containing a pyrrolyl anionic ring and a neutral imine as donor moieties [3]. The first homoleptic metal complexes of Co(II), Ni(II), Pd(II), Cu(II), and Zn(II) containing these ligands were reported in the 1960s [4]. There has been a resurgence of interest in such systems for various applications such as in catalytic organic transformations [3]. Another important focus of these ligands has been the synthesis of coordination compounds with photoluminescent and/or electroluminescent properties [5–10].

In the last few years, our group has been involved in the synthesis of a variety of metal complexes using 2-(*N*-arylimino)pyrrolyl derived ligands. In particular, we reported some luminescent zinc complexes containing 2-(*N*-arylformimino)phenanthro[9,10-*c*]pyrrolyl ligand [7], in which the π-conjugation was extended by fusing the phenanthrene ring on the pyrrolyl C3-C4 bond. We also reported the luminescent properties of several new

tetracoordinate mononuclear organoboron complexes containing 2-(*N*-arylformimino)pyrrolyl ligands, having varied the electronic and steric nature of the *N*-aryl group (Chart 1, **A**) [8]. It was found that the color of emission could be tuned from blue to bluish-green by increasing the substituent's electron-donating power. We extended our work to the synthesis of polynuclear boron complexes [9], where the iminopyrrolyl ligands have different aromatic bridging spacers (Chart 1, **B**), varying thereby the π-conjugation length and thus the color tuning range from blue to yellow. We further used a third strategy for the color tuning by extending the π-conjugation through the use of ligands containing fused aromatic fragments onto the 2-iminopyrrolyl C4-C5 or C3-C4 bonds; in fact, the employment of 2-(*N*-arylformimino)indolyl or the above mentioned 2-(*N*-arylformimino)phenanthro[9,10-*c*]pyrrolyl ligands in the coordination to boron (Chart 1, **C** and **D**) provided colors in the range blue to orange [10].

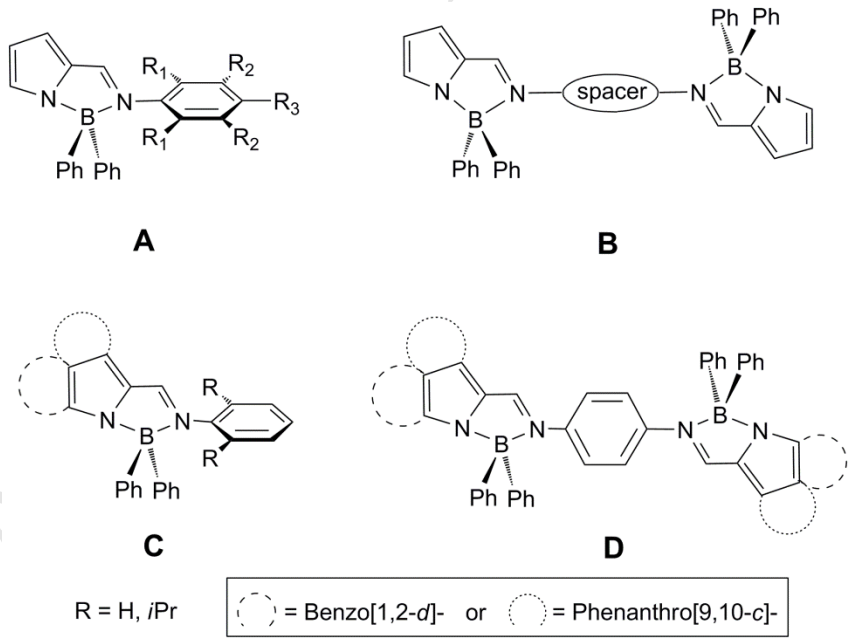


**Chart 1.**

Among the family of reported mononuclear [$BPh_2(\kappa^2N,N'$-$NC_4H_3C(H)$=N-Ar)], the complexes with bulky aryl groups, such as Ar = 2,6-$Me_2C_6H_3$ or 2,6-*i*$Pr_2C_6H_3$ (Chart 1, **A**; $R_1$ = Me or *i*Pr; $R_2$ = $R_3$ = H) gave rise to violet emission [8c], In these cases, the hindered rotation of the *N*-aryl fragment, which is unable to reach coplanarity with the 2-iminopyrrolyl fragment, reduces the π-extension of the chromophore, thus blue-shifting the emission spectra. However, the achievement of such a demanded violet emission occurs with very low fluorescence quantum efficiencies (0.5% and 2.3%, respectively, in solution), because of the extensive non-radiative quenching of the emission ($k_{nr}$ = 27.6 and 7.52 $ns^{-1}$, respectively) operating in these molecules. This efficient non-radiative decay is essentially due to the internal conversion ($k_{ic} \approx k_{nr}$) [8c].

In the present work, we describe the synthesis of a family of violet-blue emitting 2-iminopyrrolyl boron diphenyl complexes, in which significant non-radiative decay is avoided by replacing the 2,6-disubstituted *N*-aryl fragments by *N*-alkyl groups. In both the 2-iminopyrrolyl and 2-iminophenanthropyrrolyl boron chromophore frameworks, different *N*-alkyl substituents with several stereochemical features were used, in order to vary the solid state packing. The new mononuclear organoboron compounds of the types [$BPh_2(\kappa^2N,N'$-$NC_4H_3C(H)$=N-Alkyl)] and [$BPh_2(\kappa^2N,N'$-$NC_{16}H_9C(H)$=N-Alkyl)], containing 2-(*N*-aliphatic imino)pyrrolyl chelating ligands, were synthesized and characterized by multinuclear NMR, single crystal X-ray diffraction, when possible, and cyclic voltammetry. Their photophysical characterizations were performed using steady state photoluminescence (in solution and in the solid state) and time-resolved fluorescence (in solution). Density-functional theory (DFT) and time-dependent DFT (TDDFT) calculations were also carried out for these new boron complexes to determine the geometry of the ground and first excited singlet state, and to assign the nature of electronic transitions.

## 2. Results and discussion

### *2.1. Synthesis and characterization of new 2-(N-aliphatic formimino)pyrrolyl boron complexes **11-18***

The 2-(*N*-aliphatic imino)pyrrole ligand precursors **3**–**5**, **7** and **8** (Scheme 1) used in this study were synthesized and characterized according to the literature protocols [11]. The new ligand precursors **6**, **9** and **10** were also synthesized, their characterization data being presented in the experimental section.

In general, the ligand precursors $HNC_4H_3C(H)=N\text{-}CH_3$ (**3**), $HNC_4H_3C(H)=N\text{-}CH(CH_3)_2$ (**4**), $HNC_4H_3C(H)=N\text{-}C(CH_3)_3$ (**5**), $HNC_4H_3C(H)=N\text{-}CH_2(CH_2)_6CH_3$ (**6**), $HNC_4H_3C(H)=N\text{-}C_6H_{11}$ (**7**), $HNC_4H_3C(H)=N\text{-}C_{10}H_{15}$ (**8**), $HNC_{16}H_9C(H)=N\text{-}CH_3$ (**9**) and $HNC_{16}H_9C(H)=N\text{-}C_{10}H_{15}$ (**10**) were synthesized by condensation of the appropriate formyl precursors $HNC_4H_3C(H)=O$ (**1**) or $HNC_{16}H_9C(H)=O$ (**2**) with the respective aliphatic amines under reflux. The 2-formylphenanthro[9,10-*c*]pyrrole **2** was prepared by a multistep procedure, starting from phenanthrene [12].

All compounds are solids, although some with low melting points, and were characterized by $^{1}H$ and $^{13}C$ NMR spectroscopies, their spectra being consistent with those reported in the literature.

The reactions of the 2-(*N*-aliphatic imino)pyrrole chelate precursors **3**–**10** with triphenylboron ($BPh_3$) in hot toluene, overnight, under a nitrogen atmosphere, afforded the corresponding organoboron bidentate complexes **11**–**18**, which are depicted in Scheme 1.

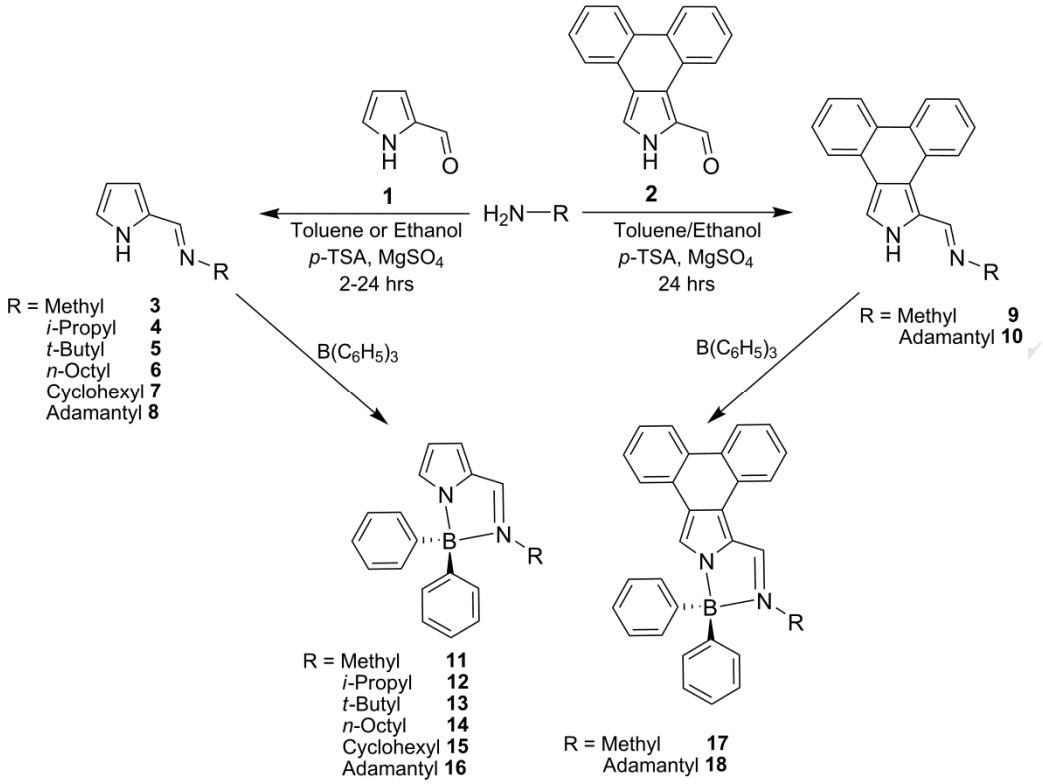


**Scheme 1.** Syntheses of the 2-(*N*-aliphatic imino)pyrrole ligand precursors **3**–**10** and the new corresponding 2-(*N*-aliphatic formimino)pyrrolyl diphenylboron complexes **11**–**18**.

The new organoboron compounds **11**–**18** are moderately air stable, and were fully characterized by $^{1}$H, $^{13}$C and $^{11}$B NMR spectroscopies (see Experimental section and Figs. S1–S30 in Supporting Information). The absence of the typical broad NH resonance in the $^{1}$H NMR spectra of the complexes confirms the anionic coordination of the pyrrolyl-*N* to the boron center. The imine proton (*H*C=N) resonances of the complexes appear as singlets in the range δ 8.04 to 8.64, downfield-shifted in relation to the respective ligand precursor, evidencing the neutral imine coordination to the boron atom. Furthermore, the $^{11}$B NMR resonance of these compounds is in the range of δ 3.61 to 7.17, confirming the formation of tetracoordinate boron compounds, being also consistent with our earlier reports [8a,c,9]. Moreover, the elemental compositions of all the complexes were determined and the results confirmed the formation of the desired products (see Experimental section). Finally, the

molecular structures of the boron complexes **14**, **15** and **18** were determined by single-crystal X-ray diffraction studies.

### *2.2. X-ray diffraction studies*

Perspective views of the molecular structures of **14**, **15** and **18** are shown in Fig. 2–4. Selected bond lengths and bond angles are given as captions in the corresponding figures. Crystals suitable for single crystal X-ray diffraction studies were obtained by cooling ethereal solutions of **14**, **15** and **18** double-layered with *n*-hexane, at -20 °C, for 2 days. Boron complexes **14** and **15** crystallized with two molecules in the unit cell, in triclinic and orthorhombic crystal systems, with *P*-1 and $Pna2_1$ space groups, respectively. Compound **16** also crystallized in the triclinic system within *P*-1 space group, showing, however, an asymmetric unit composed by one boron complex and one $Et_2O$ molecule. In the three molecular structures, the boron centers are tetracoordinate adopting typical distorted tetrahedral geometries. The *N*-aliphatic 2-iminopyrrolyl ligands chelate each boron center *via* the N1, N2 atoms to form a virtually planar five membered chelate ring in all the compounds, the remaining coordination sites being occupied by the quaternary (*ipso*) carbon atoms of two phenyl groups. The latter groups are located above and below the planes of the chelating ligand and the boron center. In addition, the B-$C_{Ph}$ distance in all complexes was found to be in the range of 1.595(10)–1.629(6) Å. The bond distances between the boron center and the two chemically different nitrogen atoms, i.e., B1-$N1_{pyrrolyl}$ of 1.565(9) and 1.571(9) (**14**), 1.561(6) and 1.566(6) (**15**) and 1.580(4) (**18**) and B1-$N2_{imine}$ of 1.614(8) and 1.619(9) (**14**), 1.605(6) and 1.615(5) (**15**), and 1.615(4) (**18**) Å, respectively, are quite comparable to the previously reported organoboron compounds [8a,c,9]. The chelating *N*,*N*' ligands exhibit bite angles N–B–N of 95.6(4)° and 94.8(5)º (**14**), 95.6(3)° and 94.9(3)º (**15**), and 95.4(2)º (**18**),

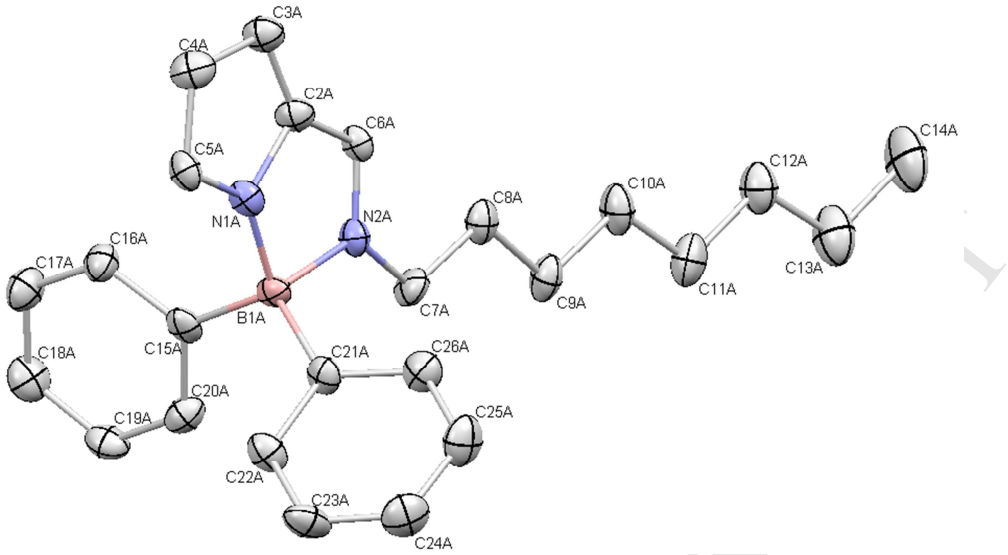


**Fig. 2.** Perspective view of the molecular structure of complex **14**. The ellipsoids were drawn at 50% probability level. All the calculated hydrogen atoms and the second molecule of the asymmetric unit were omitted for clarity. Molecule A – Selected Bond lengths (Å): B1A-N1A, 1.565(9); B1A-N2A, 1.614(8); B1A-C15A, 1.595(10); B1A-C21A, 1.607(9); C5A-N1A, 1.346(8); C2A-N1A, 1.382(8); C2A-C6A, 1.405(9); N2A-C6A, 1.302(8); N2A-C7A, 1.458(8). Selected Bond angles (°): N1A-B1A-N2A, 95.6(4); N1A-B1A-C21A, 111.0(5); N1A-B1A-C15A, 111.1(5); N2A-B1A-C15A, 107.6(5); B1A-N1A-C2A, 112.0(5); B1A-N1A-C5A, 139.9(5); B1A-N2A-C6A, 110.7(5); B1A-N2A-C7A, 123.8(5); C7A-N2A-C6A, 125.4(5); C15A-B1A-C21A, 117.7(5). Molecule B – Selected Bond lengths (Å): B1B-N1B, 1.571(9); B1B-N2B, 1.619(9); B1B-C15B, 1.615(9); B1B-C21B, 1.602(9); C5B-N1B, 1.346(8); C2B-N1B, 1.371(8); C2B-C6B, 1.418(9); N2B-C6B, 1.318(9); N2B-C7B, 1.472(8). Selected Bond angles (°): N1B-B1B-N2B, 94.8(5); N1B-B1B-C21B, 111.8(5); N1B-B1B-C15B, 112.9(5); N2B-B1B-C15B, 107.5(5); B1B-N1B-C2B, 112.9(5); B1B-N1B-C5B, 139.6(6); B1B-N2B-C6B, 111.5(5); B1B-N2B-C7B, 122.5(5); C7B-N2B-C6B, 125.9(5); C15B-B1B-C21B, 115.8(5).

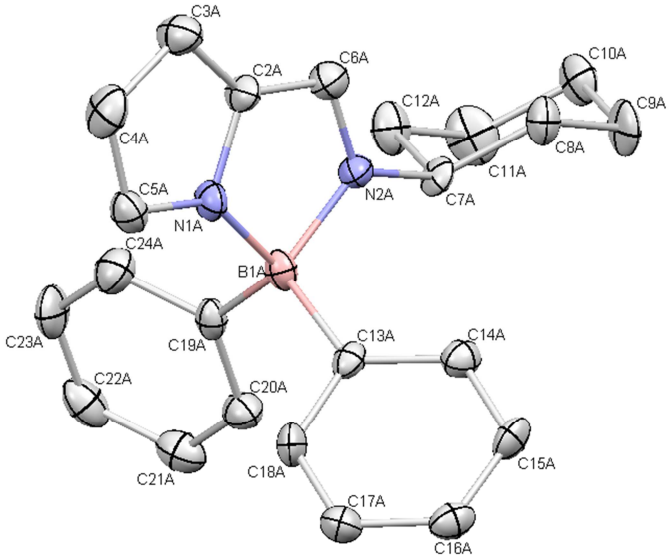


**Fig. 3.** Perspective view of the molecular structure of complex **15**. The ellipsoids were drawn at 50% probability level. All the calculated hydrogen atoms and the second molecule of the asymmetric unit were omitted for clarity. Molecule A – Selected Bond lengths (Å): B1A-N1A, 1.561(6); B1A-N2A, 1.605(6); B1A-C19A, 1.620(6); B1A-C13A, 1.605(6); N1A-C5A, 1.342(5); N1A-C2A, 1.378(5); N2A-C6A, 1.301(5); N2A-C7A, 1.476(5); C2A-C6A, 1.409(6). Selected Bond angles (°): N1A-B1A-N2A, 95.6(3); N1A-B1A-C13A, 110.8(3); N1A-B1A-C19A, 112.7(4); N2A-B1A-C13A, 112.7(4); N2A-B1A-C19A, 110.4(3); C5A-N1A-C2A, 107.8(3); C5A-N1A-B1A, 140.3(4); C6A-N2A-B1A, 111.5(3); C6A-N2A-C7A, 122.4(3); C13A-B1A-C19A, 113.4(3); B1A-N2A-C7A, 125.9(3). Molecule B – Selected Bond lengths (Å): B1B-N1B, 1.566(6); B1B-N2B, 1.615(5); B1B-C19B, 1.620(6); B1B-C13B, 1.629(6); N1B-C5B, 1.369(5); N1B-C2B, 1.347(5); N2B-C6B, 1.303(5); N2B-C7B, 1.471(5); C5B-C6B, 1.412(6). Selected Bond angles (°): N1B-B1B-N2B, 94.9(3); N1B-B1B-C13B, 111.7(4); N1B-B1B-C19B, 111.1(3); N2B-B1B-C13B, 108.5(3); N2B-B1B-C19B, 111.9(3); C5B-N1B-C2B, 107.4(3); C5B-N1B-B1B, 112.3(3); C6B-N2B-B1B, 111.6(3); C6B-N2B-C7B, 122.8(3); C13B-B1B-C19B, 116.7(3); B1B-N2B-C7B, 125.6(3).

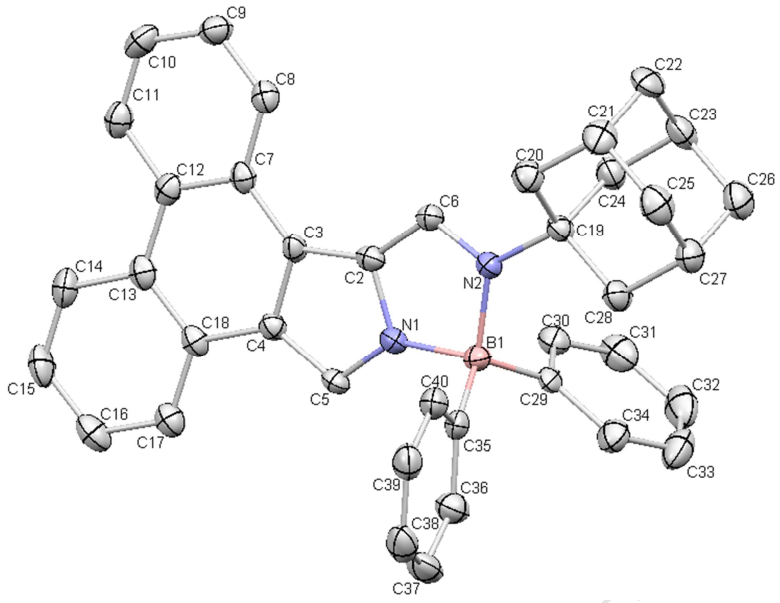


**Fig. 4.** Perspective view of the molecular structure of complex **18**. The ellipsoids were drawn at 50% probability level. All the calculated hydrogen atoms and one $Et_2O$ molecule were omitted for clarity. Selected Bond lengths (Å): B1-N1, 1.580(4); B1-N2, 1.615(4); B1-C29, 1.617(4); B1-C35, 1.613(4); N1-C5, 1.338(3); N1-C2, 1.384(3); N2-C6, 1.310(3); N2-C19, 1.503(3); C2-C6, 1.406(4). Selected Bond angles (°): N1-B1-N2, 95.4(2); N1-B1-C29, 110.7(2); N1-B1-C35, 107.2(2); N2-B1-C29, 109.8(2); N2-B1-C35, 114.0(2); C5-N1-C2, 108.8(2); C5-N1-B1, 139.1(2); C6-N2-B1, 110.6(2); C6-N2-C19, 119.7(2); C29-B1-C35, 117.5(2); B1-N2-C19, 129.2(2).

which are much smaller than the ideal bond angle (109°) for a regular tetrahedral geometry, strongly supporting the observed distortion.

The supramolecular packing of complex **14**, 2-(*N*-octylimino)pyrrolyl diphenylboron, shows, along the *a* axis, a 3D multilayer structure (see Fig. S31 in Supporting Information), formed by the aligned nonpolar aliphatic *n*-octyl chains in a bilayer type tail-to-tail arrangement. The layers are held together by C-H···π$C_{(Ar)}$ weak hydrogen bonds and π-π stacking of phenyl rings (see Fig. S32 and Table S2 in Supporting Information). Compound **15**, 2-(*N*-cyclohexylimino)pyrrolyl diphenylboron, displays weak C–H···π$C_{(Ar)}$ short contacts

(see Fig. S33 and Table S2 in Supporting Information) with no special orientation or motifs being observed. The crystal packing of **18**, 2-(*N*-adamantylimino)phenanthro[9,10-*c*]pyrrolyl diphenylboron, shows head-to-tail dimers formed by C-H···$\pi C_{(Ar)}$ short contacts and 2D-sheets containing the phenanthro[9,10-*c*]pyrrolyl-boron moieties (see Fig. S34 and Table S2 in Supporting Information), which also exhibit π-π stacking with neighboring dimers through the phenanthrenic rings of the ligands ($\pi C_{(Ar)}\cdots\pi C_{(Ar)}$, *ca.* 3.51 Å).

*2.3. Photoluminescence studies*

The UV-Vis absorption and fluorescence spectra of complexes **11**–**18** in THF are shown in Fig. 5.

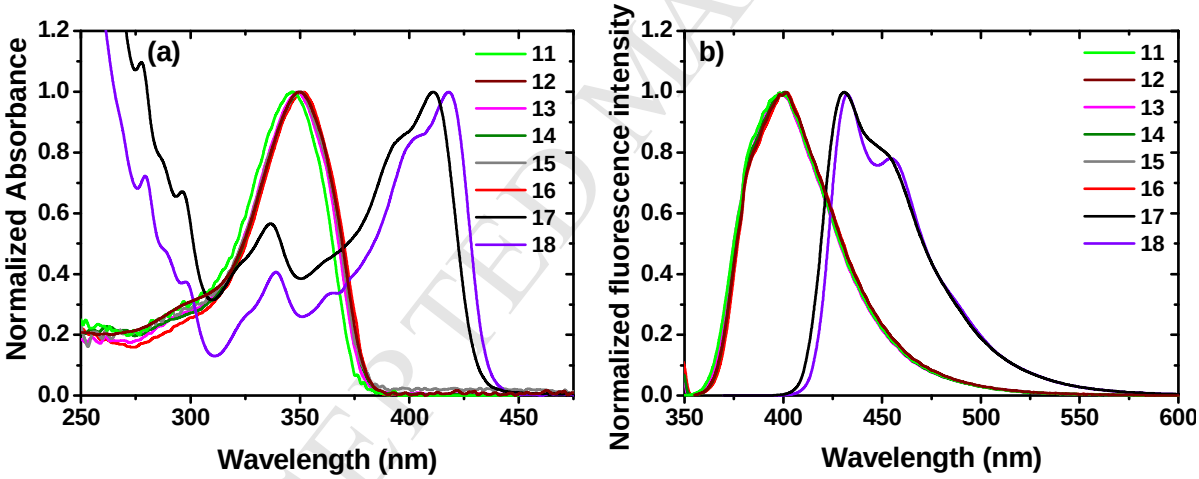


(a) (b)

**Fig. 5.** Normalized absorption (a) and emission (b) spectra of complexes **11**–**18** in THF.

The absorption spectra of 2-(*N*-alkyl formimino)pyrrolyl boron chelates **11**–**16** in THF virtually superimpose (Fig. 5a), showing very similar features, namely wavelength maxima in the range 346–352 nm, increasing with the polarizability of the aliphatic *N*-alkyl group (Table 1). The same occurs with the absorption spectra of the 2-(*N*-alkyl formimino)phenanthro-

**Table 1** Wavelength maximum ($\lambda_{abs}^{max}$) and molar extinction coefficient ($\varepsilon_{max}$) of the first absorption band, wavelength maximum ($\lambda_{em}^{max}$) and wavelength of the first vibronic transition ($\lambda_{em}^{0-0}$) of the emission band, fluorescence quantum yield ($\phi_f$), lifetime ($\tau_f$), rate constants ($k_f$), sum of non-radiative rate constants ($k_{nr}$) of the boron complexes **11**–**18**, in THF, at 293 K.

| Compound No. | Complex | $\lambda_{abs}^{max}$ (nm) | $\varepsilon_{max}$ [a] | $\lambda_{em}^{0-0}$ (nm) | $\lambda_{em}^{max}$ (nm) | $\lambda_{em}^{0-0} - \lambda_{abs}^{max}$ (nm) | $\phi_f$ | $\tau_f$ (ns) | $k_f$ [b] ($ns^{-1}$) | $k_{nr}$ [c] ($ns^{-1}$) |
|---|---|---|---|---|---|---|---|---|---|---|
| **11** | 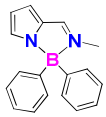 | 346 | 1.31 | 377 | 395 | 49 | 0.15 | 0.90 | 0.17 | 0.94 |
| **12** | 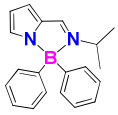 | 349 | 1.82 | 378 | 397 | 48 | 0.10 | 0.59 | 0.17 | 1.52 |
| **13** | 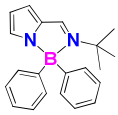 | 350 | 1.72 | 379 | 398 | 48 | 0.15 | 0.95 | 0.16 | 0.89 |
| **14** | 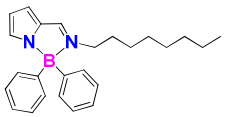 | 350 | 1.51 | 379 | 398 | 48 | 0.10 | 0.71 | 0.14 | 1.27 |
| **15** | 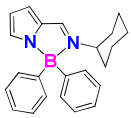 | 351 | 1.41 | 379 | 397 | 46 | 0.10 | 0.61 | 0.16 | 1.48 |
| **16** | 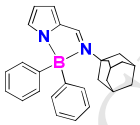 | 352 | 1.51 | 380 | 399 | 47 | 0.16 | 0.89 | 0.18 | 0.94 |
| **17** | 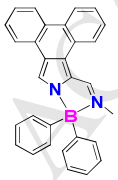 | 410 | 2.15 | 428 | 431 | 21 | 0.35 | 2.60 | 0.13 | 0.25 |
| **18** | 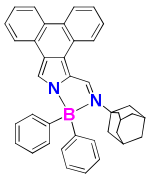 | 418 | 2.32 | 432 | 432 | 14 | 0.43 | 2.34 | 0.18 | 0.24 |

[a] $10^4$ L $mol^{-1}$ $cm^{-1}$; [b] $k_f = \phi_f / \tau_f$; [c] $k_{nr} = (1-\phi_f)/\tau_f$.

pyrrolyl boron derivatives **17** and **18**, which also exhibit maxima at very close wavelengths (410 and 417 nm, respectively), though significantly red-shifted in relation to those of **11**–**16**, owing to their higher π-conjugation length. These close similarities clearly indicate that the chromophores within each of these two families of molecules are basically the same, coinciding with the 2-iminopyrrolyl or π-extended 2-iminophenanthropyrrolyl fragments, respectively.

For the same reasons, the fluorescence spectra of each type of complexes nearly superimpose (Fig. 5b), showing wavelength maxima within 395–399 nm for the simple 2-iminopyrrolyl complexes, and 431–432 nm for the 2-iminophenanthropyrrolyl derivatives, in dilute solutions of THF. In this solvent, complexes **11**–**16** emit in the violet region (Fig. 6) with fluorescence quantum yields ($\phi_f$) varying between 0.10 and 0.16, which can be considered much higher than the efficiencies reported previously for the violet emitters [$BPh_2(\kappa^2 N,N'\text{-}NC_4H_3C(H)=N\text{-}Aryl)$] containing bulky aryl groups (2,6-$i$Pr$_2$C$_6$H$_3$ and 2,6-Me$_2$C$_6$H$_3$) [8c].

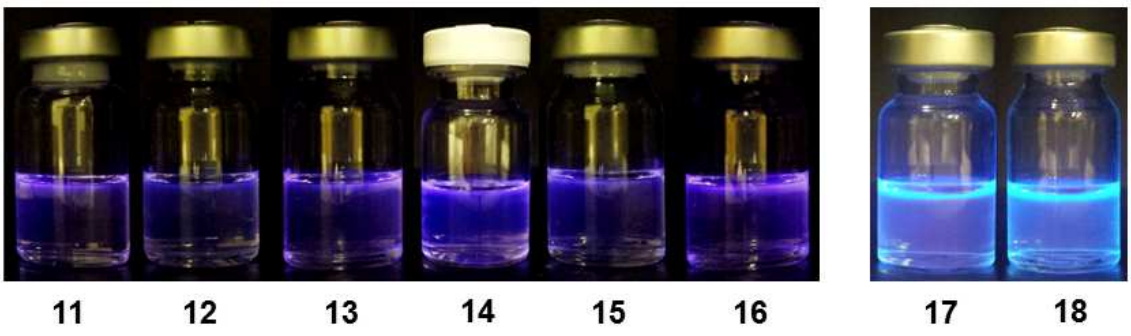


**Fig. 6.** Colors of complexes **11**–**18** in THF under UV-irradiation at 365 nm.

The fluorescence decays of all compounds **11**–**18** are single-exponentials with shorter lifetimes ($\tau_f$) for **11**–**16** (*ca.*0.6-0.9 ns) than for **17** and **18** (2.6 and 2.34 ns, respectively; column 9 in Table 1). The radiative rate constant ($k_f = \phi_f/\tau_f$) values (column 10, Table 1) of

**11**–**16** are, in fact, similar to those of the bulky *N*-aryl substituted derivatives (and others) [8c], but the corresponding non-radiative decay constants ($k_{nr}$) are 5 to 30 times lower because the *N*-alkyl groups are not intrinsically involved in the electronic transition as the *N*-aryl groups. On the other hand, the $k_{nr}$ values of **11**–**16**, and thus their fluorescence quantum yields, are similar to those measured for [$BPh_2(\kappa^2N,N'$-$NC_4H_3C(H)$=N-Aryl)] complexes containing non-bulky aryl groups substituted by electron-releasing substituents in positions 3 or 4 [8c].

Within the family **11**–**16** two subgroups may be differentiated: the one with compounds bearing more rigid *N*-alkyl groups, such as the methyl (**11**), and the tertiary *t*-butyl (**13**) and adamantyl (**16**), and the other one containing less rigid primary or secondary *N*-substituents, such as the *n*-octyl (**14**), *i*-propyl (**12**) and cyclohexyl (**15**). The latter subgroup shows higher non-radiative constants (1.27–1.52 $ns^{-1}$) than the former (0.89–0.94 $ns^{-1}$), and thus lower $\phi_f$ values (0.10 vs. 0.15-0.16).

Complexes **17** and **18**, bearing the rigid phenanthrene moiety fused on the 2-iminopyrrolyl ring, exhibit good fluorescence quantum yields (0.35 for **17** and 0.43 for **18**) and are blue emitters (Fig. 6). They show sizeable bathochromic shifts of 64 and 66 nm in relation to their corresponding simple 2-formiminopyrrolyl derivatives **11** and **16**, respectively, due to their extended π-conjugation. Their $k_f$ values are in the same order of magnitude of those of **11**–**16** but their non-radiative rate constants $k_{nr}$ are considerably lower (0.25 $ns^{-1}$ vs. 0.89–1.52 $ns^{-1}$), which is related to the higher rigidity of these extended π-conjugated fluorophores.

In summary, it is possible to set the fluorescence emission of the 2-iminopyrrolyl boron diphenyl chromophore to the violet region of the spectrum by using *N*-alkyl substituents, by limiting the π-system of the chromophore to the pyrrolyl ring and the 2-imino arm, still reaching quantum efficiencies of 10 to 15%. The fusion of a phenanthryl fragment on the C3-

C4 pyrrolyl bond of the 2-(N-alkyl formimino)pyrrolyl ring shifts the emission to the red, largely increasing the quantum efficiencies to 35–43%.

*2.4. Computational studies*

The geometries of all boron complexes **11**–**18** were optimized, based on the crystal structures of **14**, **15** and **18** described above [8,9]. The DFT [13] methodology was the same as reported before for analogous compounds, using the ADF program [14] with a BP86 functional and TZ2P basis sets for all atoms, without symmetry constraints (see also Computational details). We also optimized the geometry of the first singlet states by promoting one electron from the HOMO to the LUMO (same spin) and the geometry optimization was carried out as described for the ground state.

In the previous studies, all the boron derivatives had a phenyl substituent on the 2-iminopyrrolyl scaffold and it was shown that the dihedral angle α (Chart 2), associated with the planarity of the bidentate ligand, changed upon excitation to the singlet excited state, being therefore of major relevance in the definition of the photophysical properties. Although the phenyl group is absent in all complexes of this work, this dihedral angle seems a suitable parameter to compare different electronic states.

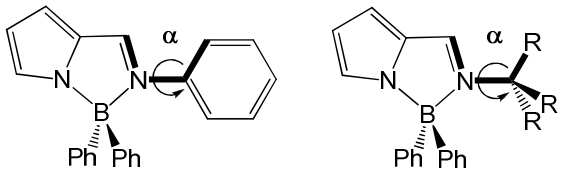


**Chart 2.**

Our analysis will address mostly four compounds (**11**, **16**-**18**), allowing the comparison of two ligands (methyl and adamantyl) and two types of π systems (2-formiminopyrrolyl and 2-

formiminophenanthropyrrolyl). In the two complexes with methyl substituents (**11** and **17**), α is 3.5° and 4.0°, respectively, in the ground state and increases to 50.1° in the singlet state in **11**, suggesting that the pyrrolyl group does not constrain rotation, while it only reaches 35.5° in **17**. In the adamantyl complexes, the ground state α angles are 48.9° and 47.0°, increasing only to 54.8° and 52.5° in the singlet state, for **16** and **18**, respectively. The bulkiness of the adamantyl prevents a different orientation in the ground state, so that the angle barely change upon reaching the singlet state. The same angles in the crystal structures described above are 53.87° (**18**) and 3.05° for **14** (*n*-octyl, a good model for methyl **11**). This contrasting behavior parallels the different photophysical properties of the two groups of complexes.

The absorption spectra of all the complexes were obtained from TDDFT calculations [15], using the implementation in ADF [14], with the BP86 functional and a TZ2P basis set, as in the geometry optimization, both in gas phase and in solvent (COSMO in ADF), and also with the SOPERT [16] method (spin-orbit coupling, SO, PBE0 functional and an all electron TZP basis set), which allows the calculations of excited states lifetimes (see subsection Computational Studies in the Experimental Section). Though the results should be the same, since all atoms are light, the approach with spin-orbit coupling often provides the best agreement with experimental data (maintaining the nature of the transitions) due to the use of different functional and basis set.

The lower energy absorption of the four complexes (**11**, **16-18**) is a broad band involving transitions from the HOMO, HOMO-1 and HOMO-2 to the LUMO, for the pyrrolyl derivatives **11** and **16**, and from the HOMO and HOMO-1 to the LUMO in the case of the phenanthropyrrolyl ones **17** and **18** (Fig. 7, top and bottom, respectively; Table 2). In the pyrrolyl derivatives **11** and **16**, both the HOMO and LUMO are localized in the 2-iminopyrrolyl ligand, while the HOMO-1 and HOMO-2 have their greatest contribution from the phenyl groups (one in each orbital). Therefore, the transition can be described as ILCT +

LLCT (intraligand charge transfer + ligand-to-ligand charge transfer). On the other hand, in complexes **17** and **18**, the HOMO-1 is completely localized in the phenanthropyrrolyl moiety, while the HOMO extends to the imino nitrogen. The electronic transition can therefore be assigned as IL.

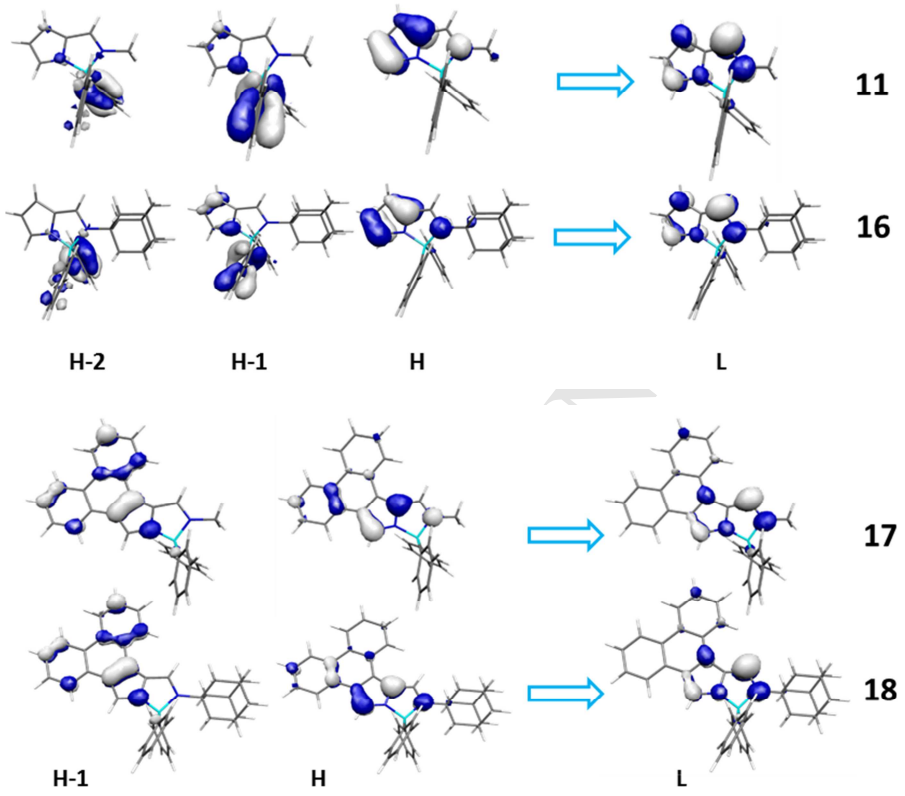


**Fig. 7.** The frontier orbitals of complexes **11**, **16** (top) and **17**, **18** (bottom) involved in the two transitions leading to the low energy absorption.

The conclusion to be taken is that the extension of the π system modifies the nature of the frontier orbitals and the transition. This has already been observed before in the boron complexes with aryl substituents at the imino nitrogen, though the effect is not exactly the same [10]. Moreover, despite the differences between methyl and adamantyl, none of their fragment orbitals contribute to the frontier orbitals and the excitations.

**Table 2** Wavelength ($\lambda$), energy ($E$), composition and oscillator strength (O.S.) of the most intense TDDFT electronic transitions calculated for complexes **11**, **16**–**18** (SO).

| Transition | $\lambda$ (nm) | $E$ (eV) | Composition | O.S. |
|---|---|---|---|---|
| **Complex 11** | | | | |
| 1 | 316 | 3.92 | H→L (64%), H-1→L (25%) | 0.151 |
| 2 | 308 | 4.02 | H-1→L (66%), H-2→L (18%), H→L (12%) | 0.056 |
| 3 | 303 | 4.08 | H-2→L (68%), H→L (20%) | 0.099 |
| **Complex 16** | | | | |
| 1 | 324 | 3.83 | H→L (71%), H-1→L (24%) | 0.196 |
| 2 | 308 | 4.02 | H-1→L (70%), H→L (17%), H-2→L (11%), | 0.109 |
| 3 | 301 | 4.11 | H-2→L (82%) | 0.058 |
| **Complex 17** | | | | |
| 1 | 376 | 3.30 | H→L (90%) | 0.260 |
| 2 | 368 | 3.37 | H-1→L (90%) | 0.221 |
| **Complex 18** | | | | |
| 1 | 380 | 3.26 | H→L (93%) | 0.364 |
| 2 | 370 | 3.35 | H-1→L (93%) | 0.192 |

Although the difference is not very relevant, two subgroups were identified with the complexes **11-16**. Since we analyzed **11** and **16**, and saw that their frontier orbitals and electronic transitions showed no difference, we also looked at one of the others, the isopropyl derivative **12**. The dihedral angle α defined in Chart 2 surprisingly decreases a little, from 69.4° to 64.9°. The lowest energy absorption is calculated in relatively good agreement with experimental values (Fig. S35, Table S3), as for the complexes **11** and **16-18** (Table 3 and Fig. 7). Only two transitions are responsible for the broad band calculated at 3.97 eV (312 nm) and both start either at the HOMO, HOMO-1, or HOMO-2, ending in the LUMO as in complexes **11** and **16**, being also assigned as mixed ILCT and LLCT. The HOMO-2 is similar to that of **11** and **16** (Fig. 7), with a stronger contribution from the two phenyl groups.

**Table 3.** Experimental wavelength maxima ($\lambda_{abs}^{max}$) of the first absorption band, absorption energies ($E_{abs}^{max}$(exp)), wavelength maxima ($\lambda_{em}^{max}$) of the emission bands, and fluorescence rate constants ($k_f$). Calculated (TDDFT) absorption energies ($E_{abs}^{max}$(GP), $E_{abs}^{max}$(SO)), wavelength maxima ($\lambda_{em}^{max}$(THF)) of the emission band, and fluorescence rate constants ($k_f$ (SO)) of the boron complexes **11**–**18**.

| Compound No. | Complex | $\lambda_{abs}^{max}$ (nm) | $E_{abs}^{max}$(exp) (eV) | $E_{abs}^{max}$(GP) (eV) | $E_{abs}^{max}$(SO) (eV) | $\lambda_{em}^{max}$ (nm) | $\lambda_{em}^{max}$(THF) (nm, eV) | $k_f$ [a] ($ns^{-1}$) | $k_f$(SO) ($ns^{-1}$) |
|---|---|---|---|---|---|---|---|---|---|
| **11** | 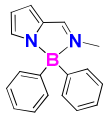 | 346 | 3.58 | 3.76 | 4.02 | 395 | 522<br>2.38 | 0.17 | 0.10 |
| **12** | 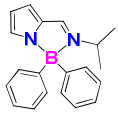 | 349 | 3.55 | 3.74 | 3.97 | 397 | 516<br>2.40 | 0.17 | 0.11 |
| **13** | 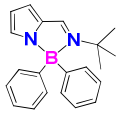 | 350 | 3.54 | 3.76 | 3.97 | 398 | 503<br>2.46 | 0.16 | 0.09 |
| **14** | 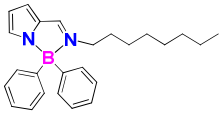 | 350 | 3.54 | 3.77 | 4.01 | 398 | 521<br>2.38 | 0.14 | 0.16 |
| **15** | 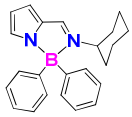 | 351 | 3.53 | 3.73 | 3.94 | 397 | 538<br>2.31 | 0.16 | 0.14 |
| **16** | 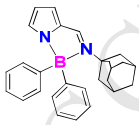 | 352 | 3.52 | 3.73 | 3.94 | 399 | 527<br>2.35 | 0.18 | 0.13 |
| **17** | 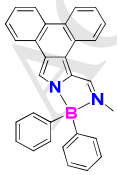 | 410 | 3.02 | 2.93 | 3.34 | 431 | 595<br>2.08 | 0.13 | 0.12 |
| **18** | 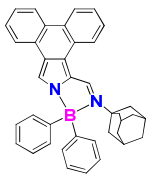 | 418 | 2.97 | 2.98 | 3.93 | 432 | 604<br>2.05 | 0.18 | 0.17 |

[a] $k_f = \phi_f / \tau_f$

The emissions directly calculated from the difference between the energy of the first singlet excited state, obtained by promoting one electron from the HOMO to the LUMO and optimizing, and the energy of the ground state with the same geometry, reproduce the experimental trends. The emissions from **17** and **18** occur at higher wavelengths than emissions from **11** and **16**, though the absolute values are shifted.

### *2.5. Electrochemical Studies*

The electrochemical properties, namely the ionization potential (IP) and the electron affinity (EA) of the complexes **11**–**18** were investigated by cyclic voltammetry. These measurements were performed in dichloromethane solutions with tetrabutylammonium tetrafluoroborate as electrolyte salt, at room temperature and under inert ($N_2$) atmosphere. The IP and EA values (Table 2) were determined from the measured reduction and oxidation onset potentials, after being converted to the absolute scale, using $Fc/Fc^+$ (ferrocene/ferrocenium ion redox couple) as external reference [8a]. As the energy level of $Fc/Fc^+$ (ferrocene/ferrocenium ion redox couple) is at 4.80 eV below the vacuum level we calculate IP (-HOMO) (eV) = $E_{onset,ox}$ (eV) + (4.80-$E_{Fc/Fc+}$) and EA (eV) = $E_{onset,red}$ (eV) + (4.80- $E_{Fc/Fc+}$) where $E_{Fc/Fc+}$ represents the half-wave potential of $Fc/Fc^+$ measured in the investigated solvent media under our setup. The values obtained are summarized in Table 4 (see also cyclic voltammograms in Figs. S36–S43 in Supporting Information), along with the energies of the HOMOs and LUMOs of the corresponding complexes calculated by DFT with solvent correction (THF).

As expected, the values of –IP correlate relatively well with the energies of the HOMOs, with the IP values differing between 0.18 and 0.27 eV from the calculated ones (see Fig. S44a in ESI). The –EA values also correlate well with the calculated LUMO energies, with differences varying between 0.03 and 0.27 eV (see Fig. S44b in ESI).

**Table 4.** Ionization potentials (IP), electron affinities (EA) of complexes **11**–**18**, estimated from cyclic voltammetry measurements, and corresponding energies of HOMOs and LUMOs, determined by DFT (THF).

| Complexes | Cyclic Voltammetry | | DFT (THF) | |
|---|---|---|---|---|
| | IP (eV) | EA (eV) | $E_{HOMO}$ (eV) | $E_{LUMO}$ (eV) |
| **11** | 5.67 | 2.53 | -5.406 | -2.493 |
| **12** | 5.63 | 2.34 | -5.409 | -2.487 |
| **13** | 5.62 | 2.34 | -5.388 | -2.513 |
| **14** | 5.65 | 2.35 | -5.381 | -2.512 |
| **15** | 5.60 | 2.32 | -5.372 | -2.511 |
| **16** | 5.60 | 2.36 | -5.346 | -2.500 |
| **17** | 5.40 | 2.59 | -5.215 | -2.777 |
| **18** | 5.39 | 2.52 | -5.171 | -2.791 |

*2.6. Electroluminescent properties*

Non-doped single-layer light-emitting diodes (LEDs) with the structure ITO/PEDOT:PSS/complex/LiF/Al were prepared and characterized for all complexes except for **12**. The films of the complexes were prepared by spin coating. In the series **11**–**16**, we could not obtain LEDs with reasonable performances. The best device with **11** gave a maximum luminance of 1 cd $m^{-2}$, and that based on **14** gave 18 cd $m^{-2}$. The remaining ones (**13**, **15** and **16**) showed negligible light emission. Conversely, OLEDs based on **17** and **18** showed reasonable performances (as shown in Fig. 8), with a maximum luminance of 69 and 88 cd $m^{-2}$, respectively, and with a maximum luminous efficiency of 0.041 and 0.019 cd $A^{-1}$,

respectively. Nevertheless, their emission is strongly controlled by aggregation, which is consistent with the observation of a dimeric supramolecular structure, involving π- π stacking, in the X-ray packing of complex **18** (see above in subsection "X-ray diffraction studies"). The recorded electroluminescence (EL) spectra are compared with the solution and film photoluminescence spectra in Fig. 9. The EL maximum occurs at 630 nm for the device based on **17**, and at 625 nm for that based on **18**, while their solution emission maxima occur at 431 nm and 432 nm, respectively. The EL spectra appear to be extended to shorter wavelengths, showing higher energy tails, which are attributed to the emission of the residual "isolated" complexes. The photoluminescence (PL) spectra recorded for the spin coated films are similar to the EL ones. In case of complex **17**, we also recorded the PL spectrum of a sublimed film, where two main emission bands are observed, with intensity maxima at 527 and 621 nm, which may be attributed to different types of aggregates and a residual emission from disordered complexes. This behavior shows that the film preparation details have a significant effect on the films photoluminescence, which is consistent with aggregation. It is worth mentioning that, upon naked eye inspection, while the sublimed film of **17** was clear and homogeneous, that prepared by spin coating was somewhat heterogeneous with macroscopic aggregates, having the spin coated films of **18** a similar appearance.

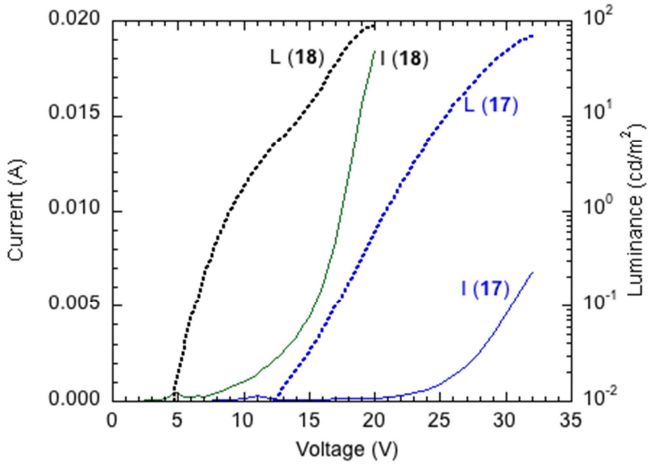


**Fig. 8.** Current (I) and luminance (L) of the devices based on **17** and **18** as function of the applied voltage.

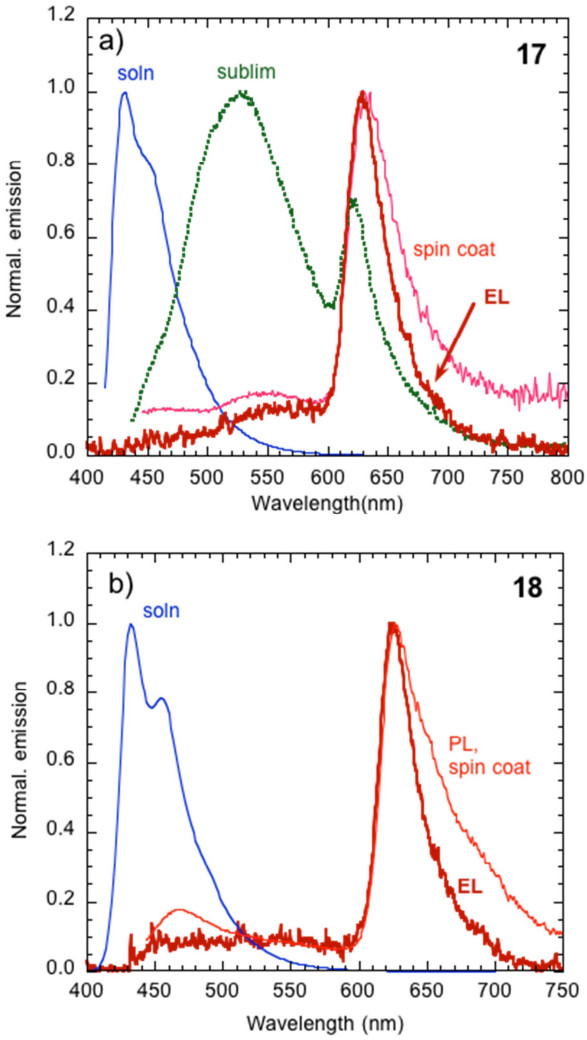


**Fig. 9.** Electroluminescence (EL) spectra of (a) **17** and (b) **18** compared to their photoluminescence (PL) spectra in THF solutions and in films prepared by spin-coating and, for the case of complex **17**, also by sublimation (sublim).

Compounds **17** and **18** exhibit similar fluorescence quantum yields and similar HOMO and LUMO energies, all determined in solution, yet device performance is significantly different, as shown in Fig. 8. In particular, the LED based on **17** shows a higher light-onset voltage and a much lower current. This, we believe, is due to a stronger detrimental effect of the aggregation on the charge transport as a minimum balanced current (electrons and holes) is required to lead to measurable light emission. Aggregation will definitely modify also the HOMO and LUMO energies with respect to the solution situation, and therefore the charge

injection barriers. However, based on the available data, we cannot compare such effects for both compounds.

This behavior shows that the film preparation details have a significant effect on the films photoluminescence and also on the LEDs performance, which is consistent with aggregation.

In conclusion, the aggregation of these boron complexes has a strong effect on their EL emission spectrum and efficiency. Their blending, for instance with conjugated polymers with adequate frontier levels energy, is expected to prevent or strongly suppress their aggregation and thereby improve the performance of the LEDs.

## 3. Conclusion

The synthesis of new mononuclear violet or blue emitting 2-iminopyrrolyl boron diphenyl complexes, containing either the 2-(*N*-alkylformimino)pyrrolyl (**11**–**16**) or the more π-extended 2-(*N*-alkylformimino)phenanthro[9,10-*c*]pyrrolyl ligands (**17** and **18**), respectively, with *N*-alkyl groups possessing different stereochemical features, was achieved in good yields. The simple 2-iminopyrrolyl boron violet emitters **11**–**16** showed fluorescence quantum yield values in the range $\phi_f$ = 0.10 – 0.16, though significantly larger than those previously reported for related violet emitters [$BPh_2(\kappa^2N,N'\text{-}NC_4H_3C(H)=N\text{-}Ar)$] containing bulky aryl groups, such as Ar = 2,6-$Me_2C_6H_3$ or 2,6-*i*$Pr_2C_6H_3$ (structure **A** in Chart 1, with $R_1$ = Me or *i*Pr, and $R_2$ = $R_3$ = H) ($\phi_f$ = 0.005 and 0.023, respectively, in THF solution), which presented extensive non-radiative processes ($k_{nr}$ = 27.6 and 7.52 $ns^{-1}$, respectively) [8c]. Conversely, the corresponding π-extended 2-iminophenanthropyrrolyl blue emitters **17** and **18**, showed enhanced quantum yields ($\phi_f$ = 0.35 and 0.43, respectively, in THF solution). This different behavior is associated with the lowest energy absorption, being ILCT + LLCT (intraligand

charge transfer + ligand-to-ligand charge transfer) in complexes **11**–**16**, involving also the phenyl groups, and simply ILCT in complexes **17** and **18**.

Non-doped single-layer electroluminescent devices were fabricated using these compounds as both emitter and ambipolar charge-transporting materials. In general, complexes **11**–**16** led to OLEDs with poor or negligible performances, complex **14** giving rise to the best device with a maximum luminance of 18 cd $m^{-2}$. Conversely, OLEDs based on **17** and **18** showed reasonable performances, with a maximum luminance of 69 and 88 cd $m^{-2}$, respectively, and maximum luminous efficiencies of 0.041 and 0.019 cd $A^{-1}$, respectively. Nevertheless, their emission is strongly controlled by aggregation, which is clearly observed by the presence of highly red-shifted emission bands in the electroluminescence (EL) spectra in relation to those of the "isolated" complexes.

## 4. Experimental section

### *4.1. General Procedures*

All experiments dealing with air- and/or moisture-sensitive materials were carried out under inert atmosphere using a dual vacuum/nitrogen line and standard Schlenk techniques. Nitrogen gas was supplied in cylinders by Air Liquide and purified by passage through 4 Å molecular sieves. Unless otherwise stated, all reagents were purchased from commercial suppliers (e.g., Acrös, Alfa Aesar, Aldrich, Fluka) and used without further purification. All solvents to be used under inert atmosphere were thoroughly deoxygenated and dehydrated before use. They were dried and purified by refluxing over a suitable drying agent followed by distillation under nitrogen. The following drying agents were used: sodium (for toluene, diethyl ether, and tetrahydrofuran (THF)), calcium hydride (for *n*-hexane and

dichloromethane). Solvents and solutions were transferred using a positive pressure of nitrogen through stainless steel cannulae and mixtures were filtered in a similar way using modified cannulae that could be fitted with glass fiber filter disks.

Nuclear magnetic resonance (NMR) spectra were recorded on Bruker Avance III 300 or Bruker Avance III 400 ($^{1}$H, $^{13}$C and $^{11}$B) spectrometers. Deuterated solvents were dried by storage over 4 Å molecular sieves and degassed by the freeze-pump-thaw method. Spectra were referenced internally using the residual protio solvent resonance relative to tetramethylsilane (δ=0). All chemical shifts are quoted in δ (ppm) and coupling constants given in hertz. Multiplicities were abbreviated as follows: broad (br), singlet (s), doublet (d), triplet (t), quartet (q), heptet (h) and multiplet (m). For air- and/or moisture sensitive materials, samples were prepared in J. Young NMR tubes in a glove box. Elemental analyses were obtained from the IST elemental analysis services.

The ligand precursors, $HNC_4H_3C(H)=N\text{-}CH_3$ (**3**), $HNC_4H_3C(H)=N\text{-}CH(CH_3)_2$ (**4**), $HNC_4H_3C(H)=N\text{-}C(CH_3)_3$ (**5**), $HNC_4H_3C(H)=N\text{-}C_6H_{11}$ (**7**) and $HNC_4H_3C(H)=N\text{-}C_{10}H_{15}$ (**8**), were synthesized according to adapted literature procedures (see Scheme 1 and general procedure below) [11].

### *4.2. Syntheses*

#### *4.2.1. General procedure for the syntheses of N,N' chelate ligand precursors **6**, **9** and **10***

In a round-bottom flask, fitted with a condenser and a $CaCl_2$ guard tube, an equimolar ratio of 2-formylpyrrole (**1**) or 2-formylphenanthro[9,10-*c*]pyrrole (**2**) and of the corresponding aliphatic amine, with a catalytic amount of *p*-toluenesulfonic acid, were suspended in absolute ethanol or toluene (20 mL). The mixture was stirred between 23–50 °C for about 2-48 hours

turning to a yellow-orange solution. All the volatiles were removed and the residue recrystallized to obtain the corresponding ligand precursors in moderate yields.

*4.2.1.1. Synthesis of $HNC_4H_3C(H)=N\text{-}CH_2(CH_2)_6CH_3$ (**6**)*

In the same manner as described above, ligand precursor **6** was obtained from the reaction between 2-formypyrrole (**1**) (0.380 g, 4 mmol) and octylamine (0.516 g, 4 mmol) with stirring at 50 °C, for 24 hrs. All the volatiles were removed and the light brown solid was recrystallized with *n*-hexane or ethanol. Yield: 0.444 g (52%). $^1$H NMR (300 MHz, $CDCl_3$): δ 8.04 (s, 1H, C*H*=N), 6.89 (s, 1H, *Pyrr*), 6.49 (dd, $J_{HH}$ = 3.4, 1.1 Hz, 1H, *Pyrr*), 6.25-6.23 (m, 1H, *Pyrr*), 3.51 (t, $J_{HH}$ = 6.9 Hz, 2H, N-C$H_2$), 1.67-1.58 (m, 2H, C$H_2$), 1.34-1.26 (m, 10H, C$H_2$), 0.88 (t, $J_{HH}$ = 6.5 Hz, 3H, C$H_3$). $^{13}$C{$^1$H} NMR (75 MHz, $CDCl_3$): δ 151.5, 130.0, 122.5, 114.8, 110.0, 60.6, 32.0, 31.3, 29.5, 29.4, 27.4, 22.8, 14.2. Anal. Calcd (%) for $C_{13}H_{22}N_2 \cdot 0.5\ C_2H_5OH$: C, 73.31; H, 10.99; N, 12.21. Found: C, 73.64; H, 11.31; N, 12.57.

*4.2.1.2. Synthesis of $HNC_{16}H_9C(H)=N\text{-}CH_3$ (**9**)*

In the same manner as described above, ligand precursor **9** was obtained by utilizing **2** (0.490 g, 2 mmol) and methylamine (33% in ethanol) (0.181 g, 2 mmol) suspended in 20 mL of toluene in a closed J. Young ampoule, and stirred at 60 °C, for 24 hrs. The mixture was cooled, filtered and all the volatiles were evaporated. The light brown solid was used as such after vacuum dried or recrystallized with ethanol. Yield: 0.131 g (61%). $^1$H NMR (300 MHz, $CDCl_3$): δ 8.98 (s, 1H, C*H*=N), 8.57-8.46 (m, 2H, *Phen*), 8.28-8.25 (m, 1H, *Phen*), 8.06-8.03 (m, 1H, *Phen*), 7.74 (s, 1H, *Phen*), 7.57-7.44 (m, 4H, *Phen*), 3.61 (s, 3H, C$H_3$). $^{13}$C{$^1$H} NMR (75 MHz, $CDCl_3$): δ 153.1, 130.5, 128.7, 128.4, 127.4, 127.2, 125.9, 125.5, 125.4, 124.3,

124.1, 123.6, 123.1, 122.2, 120.5, 115.8, 47.3. Anal. Calcd (%) for $C_{18}H_{14}N_2 \cdot 0.25\ C_2H_5OH$: C, 82.35; H, 5.79; N, 10.38. Found: C, 82.80; H, 5.52; N, 10.71.

*4.2.1.3. Synthesis of $HNC_{16}H_9C(H)=N\text{-}C_{10}H_{15}$ (**10**)*

The reaction was performed according to the procedure described for **6**, utilizing **2** (0.245 g, 1 mmol) and adamantylamine (0.151 g, 1 mmol), affording ligand precursor **10**. The brown solid was used as such after vacuum dried or recrystallized with ethanol. Yield: 0.215 g (57%). $^1$H NMR (300 MHz, $CDCl_3$): δ 8.77 (s, 1H, C*H*=N), 8.59 (br, 1H, *Phen*), 8.52 (d, $J_{HH}$ = 4.3 Hz, 1H, *Phen*), 8.20 (br, 1H, *Phen*), 8.12 (d, $J_{HH}$ = 3.7 Hz, 1H, *Phen*), 7.97 (d, $J_{HH}$ = 1.7 Hz, 1H, *Phen*), 7.56 – 7.49 (m, 4H, *Phen*), 2.24 (s, 3H, adamantyl-C*H*), 1.96 (s, 6H, adamantyl-C*H*$_2$), 1.81 – 1.73 (m, 6H, adamantyl-C*H*$_2$). $^{13}$C{$^1$H} NMR (75 MHz, $CDCl_3$): δ 144.6, 130.6, 128.6, 128.5, 128.4, 127.3, 127.2, 127.1, 126.0, 125.9, 125.3, 125.0, 124.4, 124.3, 123.6, 123.5, 123.14, 56.5, 43.6, 36.4, 29.7. Anal. Calcd (%) for $C_{27}H_{26}N_2 \cdot 0.5\ C_2H_5OH$: C, 84.69; H, 7.11; N, 7.18. Found: C, 84.92; H, 7.14; N, 6.54.

*4.2.2. General procedure for syntheses of new organoboron complexes* **11**–**18**

In a typical experiment, equimolar proportions of triphenylboron and the desired 2-iminopyrrolyl ligand precursor, dissolved in 25 mL of toluene, were heated to reflux overnight (16–20 h), under nitrogen atmosphere (Scheme 1). The reaction mixture was cooled to room temperature and all the volatiles were evaporated. The residue was extracted with the appropriate solvent, such as *n*-hexane or $Et_2O$, in about 5–10 mL and, if needed in the latter case, double layered with *n*-hexane. The resulting solution was kept at -20 °C to afford the corresponding boron complexes **11**–**18**.

*4.2.2.1. Synthesis of [B(C$_6$H$_5$)$_2$(κ$^2$N,N'-NC$_4$H$_3$C(H)=N-CH$_3$)] (**11**)*

According to the general procedure described above, a mixture of **3** (0.216 g, 2 mmol) and B(C$_6$H$_5$)$_3$ (0.484 g, 2 mmol) was used, resulting in complex **11** as a pale brown solid. The pure microcrystalline complex was obtained by extraction with Et$_2$O, followed by double layering with *n*-hexane and storage of the resulting solution at -20 °C. Yield: 0.359 g (66%). $^1$H NMR (300 MHz, CD$_2$Cl$_2$): δ 8.04 (s, 1H, C*H*=N), 7.30 – 7.19 (m, 10H, B-*Ph*), 7.11 (s, 1H, *Pyrr*), 6.83 (d, $J_{HH}$ = 3.7 Hz, 1H, *Pyrr*), 6.46 (dd, $J_{HH}$ = 3.4 Hz, $J_{HH}$ = 1.8 Hz, 1H, *Pyrr*), 3.35 (s, 3H, C*H*$_3$). $^{13}$C{$^1$H} NMR (75 MHz, CD$_2$Cl$_2$): δ 155.0, 146.1 (br), 133.9, 133.2, 130.0, 128.0, 127.0, 115.6, 112.3, 37.7. $^{11}$B NMR (96.29 MHz, CD$_2$Cl$_2$): δ 3.63. Anal. Calcd (%) for C$_{18}$H$_{17}$BN$_2$: C, 79.44; H, 6.30; N, 10.29. Found: C, 79.36; H, 6.27; N, 10.26.

*4.2.2.2. Synthesis of [B(C$_6$H$_5$)$_2$(κ$^2$N,N'-NC$_4$H$_3$C(H)=N-CH(CH$_3$)$_2$)] (**12**)*

According to the general procedure described above, a mixture of **4** (0.328 g, 2.4 mmol) and B(C$_6$H$_5$)$_3$ (0.580 g, 2.4 mmol) afforded complex **12** as a brown sticky solid. The pure microcrystalline complex was obtained by extraction with *n*-hexane and storage of the resulting solution at -20 °C. Yield: 0.367 g (51%). $^1$H NMR (300 MHz, CD$_2$Cl$_2$): δ 8.24 (s, 1H, C*H*=N), 7.31 – 7.20 (m, 10H, B-*Ph*), 7.10 – 7.09 (m, 1H, *Pyrr*), 6.84 (dd, $J_{HH}$ = 3.7 Hz, $J_{HH}$ = 0.8 Hz, 1H, *Pyrr*), 6.48 (dd, $J_{HH}$ = 3.7 Hz, $J_{HH}$ = 2.0 Hz, 1H, *Pyrr*), 4.12 – 3.99 (m, 1H, C*H*-(CH$_3$)$_2$), 1.14 (d, $J_{HH}$ = 6.7 Hz, 6H, C*H*$_3$). $^{13}$C{$^1$H} NMR (75 MHz, CD$_2$Cl$_2$): δ 151.5, 147.3 (br), 134.5, 133.4, 129.4, 127.9, 127.0, 115.6, 112.1, 49.8, 24.1. $^{11}$B NMR (96.29 MHz, CD$_2$Cl$_2$): δ 3.92. Anal. Calcd (%) for C$_{20}$H$_{21}$BN$_2$: C, 80.02; H, 7.05; N, 9.33. Found: C, 79.90; H, 7.20; N, 9.39.

*4.2.2.3. Synthesis of [B($C_6H_5$)$_2$($\kappa^2$N,N'-$NC_4H_3C(H)$=N-$C(CH_3)_3$)] (**13**)*

In the same manner as described above, a mixture of **5** (0.300 g, 2 mmol) and B($C_6H_5$)$_3$ (0.484 g, 2 mmol) afforded complex **13** as a brown sticky solid. The pure microcrystalline complex was obtained by extraction with *n*-hexane storage of the resulting solution at -20 °C. Yield, 0.346 g (55%). $^1$H NMR (300 MHz, $CD_2Cl_2$): δ 8.44 (s, 1H, C*H*=N), 7.41 – 7.38 (m, 4H, B-*Ph*), 7.31 – 7.22 (m, 6H, B-*Ph*), 6.87 (s, 1H, *Pyrr*), 6.82 (d, $J_{HH}$ = 3.6 Hz, 1H, *Pyrr*), 6.41 (br, 1H, *Pyrr*), 1.30 (s, 9H, C$H_3$). $^{13}$C{$^1$H} NMR (75 MHz, $CD_2Cl_2$): δ 154.0, 147.6 (br), 134.1, 133.4, 128.6, 127.8, 126.8, 115.9, 112.1, 59.4, 31.3. $^{11}$B NMR (96.29 MHz, $CD_2Cl_2$): δ 4.47. Anal. Calcd (%) for $C_{21}H_{23}BN_2$: C, 80.27; H, 7.38; N, 8.91. Found: C, 80.04; H, 7.51; N, 8.89.

*4.2.2.4. Synthesis of [B($C_6H_5$)$_2$($\kappa^2$N,N'-$NC_4H_3C(H)$=N-$CH_2(CH_2)_6CH_3$)] (**14**)*

In the same manner as described above, a mixture of **6** (0.206 g, 1 mmol) and B($C_6H_5$)$_3$ (0.242 g, 1 mmol) afforded complex **14** as brown solid. The pure complex was obtained by extraction with $Et_2O$ followed by double layering with *n*-hexane and storage of the resulting solution at -20 °C. Prism brown crystals suitable for single crystal X-ray diffraction studies were obtained from the mixture. Yield: 0.215 g (58%). $^1$H NMR (300 MHz, $CD_2Cl_2$): δ 8.12 (s, 1H, C*H*=N), 7.29 – 7.18 (m, 10H, B-*Ph*), 7.08 (brs, 1H, *Pyrr*), 6.82 (dd, $J_{HH}$ = 3.7, 0.6 Hz, 1H, *Pyrr*), 6.46 (dd, $J_{HH}$ = 3.7 Hz, $J_{HH}$ = 2.0 Hz, 1H, *Pyrr*), 3.59 (t, $J_{HH}$ = 7.5 Hz, 2H, N-C$H_2$), 1.48 – 1.39 (m, 2H, C$H_2$), 1.30 – 1.15 (m, 10H, C$H_2$), 0.87 (t, $J_{HH}$ = 6.9 Hz, 3H, C$H_3$). $^{13}$C{$^1$H} NMR (75 MHz, $CD_2Cl_2$): δ 153.3, 146.4 (br), 134.2, 133.3, 129.5, 128.0, 127.0, 115.6, 112.1, 49.8, 32.1, 29.9, 29.4, 27.0, 23.0, 14.2. $^{11}$B NMR (96.29 MHz, $CD_2Cl_2$): δ 3.68.

Anal. Calcd (%) for $C_{25}H_{31}BN_2$: C, 81.08; H, 8.44; N, 7.56. Found: C, 81.19; H, 8.68; N, 7.52.

*4.2.2.5. Synthesis of [B(C$_6$H$_5$)$_2$(κ$^2$N,N'-NC$_4$H$_3$C(H)=N-C$_6$H$_{11}$)] (***15***)*

In the same manner as described above, a mixture of **7** (0.352 g, 2 mmol) and $B(C_6H_5)_3$ (0.484 g, 2 mmol) afforded complex **15** as a pale yellow solid. The pure complex was obtained by extraction with $Et_2O$ followed by double layering with *n*-hexane and storage of the resulting solution at -20 °C. Yellow crystals suitable for single crystal X-ray diffraction studies were obtained from the mixture. Yield: 0.567 g (83%). $^1$H NMR (400 MHz, $CD_2Cl_2$): δ 8.20 (s, 1H, C*H*=N), 7.28 – 7.21 (m, 10H, B-*Ph*), 7.07 (s, 1H, *Pyrr*), 6.82 (d, $J_{HH}$ = 3.7 Hz, 1H, *Pyrr*), 6.47 – 6.46 (m, 1H, *Pyrr*), 3.61 (t, $J_{HH}$ = 11.7 Hz, 1H, N-C*H*), 1.73 – 1.62 (m, 5H, C*H$_2$*), 1.37 – 1.12 (m, 5H, C*H$_2$*). $^{13}$C{$^1$H} NMR (100 MHz, $CD_2Cl_2$): δ 151.7, 147.0 (br), 134.5, 133.3, 129.3, 127.9, 127.0, 115.6, 112.0, 57.9, 35.1, 26.1, 25.8. $^{11}$B NMR (128 MHz, $CD_2Cl_2$): δ 3.85. Anal. Calcd (%) for $C_{23}H_{25}BN_2$: C, 81.18; H, 7.41; N, 8.23. Found: C, 81.08; H, 7.53; N, 8.31.

*4.2.2.6. Synthesis of [B(C$_6$H$_5$)$_2$(κ$^2$N,N'-NC$_4$H$_3$C(H)=N-C$_{10}$H$_{15}$)] (***16***)*

In the same manner as described above, a mixture of **8** (0.228 g, 1 mmol) and $B(C_6H_5)_3$ (0.242 g, 1 mmol) afforded complex **16** as a white solid. The pure microcrystalline complex was obtained by extraction with *n*-hexane and storage of the resulting solution at -20 °C. Yield: 0.239 g (61%). $^1$H NMR (300 MHz, $CD_2Cl_2$): δ 8.47 (s, 1H, C*H*=N), 7.39 – 7.19 (m, 10H, B-*Ph*), 6.80 – 6.77 (m, 2H, *Pyrr*), 6.37 (d, $J_{HH}$ = 1.6 Hz, 1H, *Pyrr*), 1.98 (s, 3H, adamantyl-C*H*), 1.88 (s, 6H, adamantyl-C*H$_2$*), 1.59 (d, $J_{HH}$ = 12.3 Hz, 3H, adamantyl-C*H$_2$*),

1.49 (d, $J_{HH}$ = 12.3 Hz, 3H, adamantyl-C*H*$_2$). $^{13}C\{^1H\}$ NMR (75 MHz, $CD_2Cl_2$): δ 152.3, 147.2 (br), 133.7, 132.8, 127.9, 127.2, 126.3, 115.3, 111.4, 60.1, 43.1, 35.6, 29.7. $^{11}B$ NMR (96.29 MHz, $CD_2Cl_2$): δ 4.42. Anal. Calcd (%) for $C_{27}H_{29}BN_2$: C, 82.65; H, 7.45; N, 7.14. Found: C, 81.97; H, 7.52; N, 7.18.

*4.2.2.7. Synthesis of [B(C$_6$H$_5$)$_2$(κ$^2$N,N'-NC$_{16}$H$_9$C(H)=N-CH$_3$)] (**17**)*

In the same manner as described above, a mixture of **9** (0.258 g, 1 mmol) and $B(C_6H_5)_3$ (0.242 g, 1 mmol) afforded complex **17** as a pale green solid. The pure complex was obtained by extraction with toluene, followed by double layering with *n*-hexane and storage of the resulting solution at -20 °C. Yield: 0.295 g (70%). $^1H$ NMR (300 MHz, $CD_2Cl_2$): δ 8.65 – 8.62 (m, 2H, C*H*=N + *Phen*), 8.60 – 8.56 (m, 1H, *Phen*), 8.26 – 8.23 (m, 1H, *Phen*), 8.13 – 8.10 (m, 1H, *Phen*), 8.04 (s, 1H, *Phen*), 7.64 – 7.60 (m, 2H, *Phen*), 7.55 – 7.51 (m, 2H, *Phen*), 7.31 – 7.24 (m, 10H, B-*Ph*), 3.48 (s, 3H, C*H*$_3$). $^{13}C\{^1H\}$ NMR (75 MHz, $CD_2Cl_2$): δ 153.7, 133.3, 130.3, 128.6, 128.5, 128.2, 128.1, 127.7, 127.5, 127.2, 126.8, 126.7, 125.7, 125.0, 124.4, 123.9, 123.6, 122.1, 37.8. $^{11}B$ NMR (96.29 MHz, $CD_2Cl_2$): δ 3.61. Anal. Calcd (%) for $C_{30}H_{23}BN_2$: C, 85.32; H, 5.49; N, 6.63. Found: C, 84.43; H, 5.46; N, 6.60.

*4.2.2.8. Synthesis of [B(C$_6$H$_5$)$_2$(κ$^2$N,N'-NC$_{16}$H$_9$C(H)=N-C$_{10}$H$_{15}$)] (**18**)*

In the same manner as described above, a mixture of **10** (0.215 g, 0.6 mmol) and $B(C_6H_5)_3$ (0.138 g, 0.6 mmol) afforded complex **18** as a pale green solid. The pure complex was obtained by extraction with toluene, followed by double layering with *n*-hexane or diethyl ether and storage of the resulting solution at -20 °C. Yield: 0.225 g (73%). $^1H$ NMR (400 MHz, $CD_2Cl_2$): δ 9.05 (s, 1H, C*H*=N), 8.64 – 8.62 (m, 1H, *Phen*), 8.58 – 8.54 (m, 1H, *Phen*),

8.35 (dd, $J_{HH}$ = 7.8 Hz, $J_{HH}$ = 1.2 Hz, 1H, *Phen*), 8.01 – 7.97 (m, 1H, *Phen*), 7.75 (s, 1H, *Phen*), 7.67 (td, $J_{HH}$ = 7.5 Hz, $J_{HH}$ = 1.3 Hz, 1H, *Phen*), 7.61 (td, $J_{HH}$ = 7.6 Hz, $J_{HH}$ = 1.5 Hz, 1H, *Phen*), 7.51 – 7.47 (m, 6H, B-*Ph*), 7.30 – 7.21 (m, 6H, B-*Ph* + *Phen*), 2.04 – 2.02 (m, 9H, adamantyl-C$H_2$ + adamantyl-C*H*), 1.63 (d, $J_{HH}$ = 12 Hz, 3H, adamantyl-C$H_2$), 1.56 (d, $J_{HH}$ = 12 Hz, 3H, adamantyl-C$H_2$). $^{13}C\{^1H\}$ NMR (100 MHz, $CD_2Cl_2$): δ 151.5, 147.4, 134.3, 130.3, 128.7, 128.5, 127.9, 127.6, 127.4, 127.1, 127.0, 126.6, 125.6, 125.1, 124.4, 123.8, 123.6, 123.3, 121.8, 66.1, 43.8, 36.1, 30.3. $^{11}B$ NMR (128 MHz, $CD_2Cl_2$): δ 3.94. Anal. Calcd (%) for $C_{39}H_{35}BN_2 \cdot 0.5\ C_4H_{10}O$: C, 84.96; H, 6.96; N, 4.83. Found: C, 85.23; H, 6.67; N, 5.02.

### *4.3. X-Ray data collection*

Crystallographic and experimental details of crystal structure determinations are listed in Table S1 in Supporting Information. Crystals were selected under an inert atmosphere, covered with polyfluoroether oil, and mounted on a nylon loop. Crystallographic data for complexes **14**, **15** and **18** were collected using graphite monochromated Mo-Kα radiation ($\lambda$ =0.71073 Å) on a Bruker AXS-KAPPA APEX II diffractometer equipped with an Oxford Cryosystem open-flow nitrogen cryostat, at 150 K. Cell parameters were retrieved using Bruker SMART software and refined using Bruker SAINT on all observed reflections. Absorption corrections were applied using SADABS. Structure solution and refinement were performed using direct methods with the programs SIR2004 [17] and SIR2014 [18] and SHELXL [19], included in the package of programs WINGX-Version 2014.1 [20]. All non-hydrogen atoms were refined anisotropically. All hydrogen atoms were inserted in idealized positions and allowed to refine riding on the parent carbon atom, with C–H distances of 0.95, 0.98, 0.99 and 1.00 Å for aromatic, methyl, methylene and methine H atoms, respectively, and with $U_{iso}$(H) = 1.2$U_{eq}$(C). Graphic presentations were prepared with Mercury [21]. The

supramolecular arrangements were performed based on the available information on short contacts determined by PLATON [22]. Data was deposited in CCDC under the deposit numbers 1496968 for **14**, 1496967 for **15**, and 1496966 for **18**.

### *4.4. Cyclic Voltammetry measurements*

Cyclic voltammetry (CV) measurements were performed on a Solartron potentiostat with a three-electrode cell with a 0.1 M tetrabutylammonium tetrafluorborate ($TBABF_4$)/$CH_2Cl_2$ supporting electrolyte, at a scan rate of 50 mV/s, at room temperature, and under inert ($N_2$) atmosphere. A saturated calomel electrode (SCE), a platinum wire, and a platinum disk were used as reference electrode, counter electrode, and working electrode, respectively.

### *4.5. Spectroscopic measurements*

Absorption and fluorescence spectra of **11**–**18** solutions in freshly distilled THF were run with an Agilent Cary 8454 UV-Visible spectrophotometer and a SPEX Fluorolog 212I, respectively. The fluorescence spectra were collected with right angle geometry, in the S/R mode, and corrected for instrumental wavelength dependence. Fluorescence quantum yields were determined by comparison with the quantum yields of α-terthiophene (for compounds **11** to **16**) and α-pentathiophene (for compounds **17** and **18**) in dioxane at 25 ºC.

Fluorescence decays were measured using the time-correlated single photon counting technique with a previously described home-made apparatus [23]. Briefly, the excitation pulses were provided by a Millennia Xs/Tsunami lasers system from Spectra Physics, operating at 82 MHz, and frequency-doubled. The sample emission was collected at the magic angle (Glan Thompson polarizer), passed through a monochromator (Jobin-Yvon H20

Vis), and detected with a microchannel plate photomultiplier (Hamamatsu R3809u-50). The FWHM of the instrumental response (obtained with a scattering Ludox solution) is ca. 18 ps with 814 fs/channel resolution. Pulse profile and sample emissions were collected until approximately $5\times10^3$ total counts had been accumulated at the maximum. Fluorescence decays were deconvoluted from the excitation pulse using the modulation functions method (Sand program) [24].

### *4.6. Computational Studies*

Density Functional Theory [13] calculations were performed using the Amsterdam Density Functional program package (ADF) [14]. Gradient corrected geometry optimizations, without symmetry constraints, were performed using the Local Density Approximation of the correlation energy (Vosko-Wilk-Nusair) [25], and the Generalized Gradient Approximation (Becke's [26] exchange and Perdew's [27] correlation functionals). Relativistic effects were treated with the ZORA approximation [28]. Unrestricted calculations were performed for excited singlet states. The core orbitals were frozen for B, C, and N (1s). Triple ζ Slater-type orbitals (STO) were used to describe the valence shells B, C, and N (2s and 2p). A set of two polarization functions was added to B, C, and N (single ζ, 3d, 4f). Triple ζ Slater-type orbitals (STO) were used to describe the valence shells of H (1s) augmented with two polarization functions (single ζ 2s, 2p). Time Dependent DFT [15] calculations in the ADF implementation were performed to determine the excitation energies. The solvent effect was included with the COSMO approach in ADF in single point calculations on the optimized geometries. The geometry of the excited state was calculated by promoting one electron from the HOMO to the LUMO with S=0. The perturbative method in the time-dependent density-functional theory (TDDFT) formalism with the influence of spin-orbit coupling effect

(SOPERT) [16] was used in order to calculate the excited states lifetimes. In these calculations, complete basis sets were used for all elements (same as above, without any frozen core) with the hybrid PBE0 functional [29]. We checked that the absorption spectra calculated with this approach were the same that were obtained in the same conditions without including spin-orbit coupling since all the atoms are light.

The structures were modeled after those of compounds **14**, **15** and **18** described above. Three-dimensional representations of the orbitals were obtained with Molekel [30] and electronic spectra with Chemcraft [31].

### *4.7. Light-emitting Diodes Studies*

Light-emitting diodes were prepared on glass/ITO substrates (ITO=indium-tin oxide), which were cleaned with detergent, distilled water, acetone and isopropanol. They were treated with oxygen plasma, prior to the deposition of PEDOT:PSS (poly(3,4-ethylenedioxythiophene) doped with polystyrene sulfonic acid, CLEVIOS P VP.AI 4083 from Heraeus Clevios GmbH) by spin coating. The PEDOT:PSS films (40 nm thick, as measured with a DEKTAK profilometer) were annealed in air for 2 minutes at 120 $^{o}$C, and then transferred into a nitrogen filled glove box.

Films of the complexes **11**–**18** were deposited on top of PEDOT:PSS by spin coating, from their THF solutions, inside the glove box. The complexes films thicknesses were in the range 60-80 nm. The substrates were then placed inside an evaporation chamber, and the top electrode consisting on 1.5 nm LiF and ca. 80 nm of aluminum, was deposited at a base pressure of $2\times10^{-6}$ mbar through a shadow mask, defining pixel areas of 4 mm$^2$.

Devices were tested under vacuum, using a K2400 Source Meter and a calibrated silicon photodiode, as described previously [32]. The electroluminescence (EL) spectra were

obtained with a CCD spectrograph (from Ocean Optics or from ScanSci). External quantum efficiency values were estimated as detailed in Ref. [32].

**Acknowledgements**

We thank the Fundação para a Ciência e Tecnologia, Portugal, for financial support [Projects UID/QUI/00100/2013, UID/MULTI/00612/2013, UID/EEA/50008/2013 and RECI/QEQ-QIN70189/2012] and for fellowships to K.P., B.F., C.S.B.G. and D.V.V. [SFRH/BPD/89167/2012, SFRH/BD/80122/2011, SFRH/BPD/107834/2015, and SFRH/BD/81017/2011, respectively].

**References**

[1] a) Wong TKS. Handbook of Organic Electronics and Photonics Vol. 2. In. Nalwa HS, editors. Stevenson Ranch, CA: American Scientific Publishers; 2008, p. 413–72.
b) Shen Z, Burrows PE, Bulovic V, Borrest SR, Thompson ME. Science 1997;276:2009–11.
c) Bulovic V, Gu G, Burrows PE, Forrest SR. Nature 1996;380:29.
d) Aziz H, Popovic ZD, Hu N-X, Hor A-M, Xu G. Science 1999;283:1900–2.
e) Wang S. Coord Chem Rev 2001;215:79–98.
f) Lamansky S, Djurovich P, Murphy D, Abdel-Razzaq F, Lee HE, Adachi C, et al. J Am Chem Soc 2001;123:4304 – 12.
g) Balzani V, Juris A, Venturi M, Campagna S, Serroni S. Chem Rev 1996;96,759–834.

[2] a) Suresh D, Gomes PT. The Silver/Gold Jubilee International Conference on Organometallic Chemistry Celebratory Book, 1st ed. In: Pombeiro AJL, editor. Advances in Organometallic Chemistry and Catalysis: Chap. 36. Hoboken NJ USA: Wiley; 2014, p. 485–92.
b) Li D, Zhang H, Wang Y, Chem Soc Rev 2013;42:8416–33.
c) Frath D, Massue J, Ulrich G, Ziessel R. Angew Chem Int Ed 2014;53:2290–310; Angew Chem 2014:126:2322–42.
d) Rao Y-L, Amarne H, Wang S. Coord Chem Rev 2012;256:759–70.
e) Kano N, Furuta A, Kambe T, Yoshino J, Shibata T, Kawashima T, et al. Eur J Inorg Chem 2012;1584–7.
f) Li D, Zhang Z, Zhao S, Wang Y, Zhang H. Dalton Trans 2011;40:1279–85.
g) Li D, Yuan Y, Bi H, Yao D, Zhao X, Tian W, et al. Inorg Chem 2011;50:4825–31.
h) Yoshino J, Furuta A, Kambe T, Itoi H, Kano N, Kawashima T, et al. Chem Eur J 2010;16:5026–35.
i) Amarne H, Baik C, Murphy SK, Wang S. Chem Eur J 2010;16:4750–61.
j) Zhang ZBH, Zhang Y, Yao D, Gao H, Fan Y, Zhang H, et al. Inorg Chem 2009;48:7230–6.
k) Liddle BJ, Silva RM, Morin TJ, Macedo FP, Shukla R, Lindeman SV, et al. J Org Chem 2007;72:5637–46.

l) Ugolotti J, Hellstrom S, Britovsek GJP, Jones TS, Hunt P, White AJP. Dalton Trans 2007;1425–32.

m) Yoshino J, Kano N, Kawashima T. Chem Commun 2007;559–61.

n) Kappaun S, Rentenberger S, Pogantsch A, Zojer E, Mereiter K, Trimmel G, et al. Chem Mater 2006;18:3539–47.

o) Liu Q-D, Mudadu MS, Thummel R, Tao Y, Wang S. Adv Funct Mater. 2005;15:143-54.

p) Qin Y, Pagba C, Piotrowiak P, Jäkle F. J Am Chem Soc 2004;126:7015–8.

q) Cheng C-C, Yu W-S, Chou P-T, Peng S-M, Lee G-H, Wu P-C, et al. Chem Commun 2003;2628–9.

r) Liu Y, Guo J, Zhang H, Wang Y. Angew Chem Int Ed 2002;41:182–4; Angew Chem 2002;114:190–2.

s) Wu Q, Esteghamatian M, Hu N-X, Popovic Z, Enright G, Tao Y, et al. Chem Mater 2000;12:79–83.

t) Anderson S, Weaver MS, Hudson AJ. Synth Met 2000;111–2:459–63.

u) Pais VF, Alcaide MM, López-Rodríguez R, Collado D, Nájera F, Pérez-Inestrosa E, et al. Chem Eur J. 2015;21:15369–76.

[3] a) Panda TK, Yamamoto K, Yamamoto K, Kaneko H, Yang Y, Tsurugi H, et al. Organometallics 2012;31:2268–74.

b) Mu J-S, Wang Y-X, Li B-X, Li Y-S, Dalton Trans 2011;40:3490–7.

c) Tsurugi H, Matsuo Y, Mashima K. J Mol Cat A Chem 2006;254:131–7.

d) Bellabarba RM, Gomes PT, Pascu SI. Dalton Trans 2003;4431–6.

e) Carabineiro SA, Silva LC, Gomes PT, Pereira LCJ, Veiros LF, Pascu SI, et al. Inorg Chem 2007;46:6880–90.

f) Carabineiro SA, Gomes PT, Veiros LF, Freire C, Pereira LCJ, Henriques RT, et al Dalton Trans 2007;5460–70.

g) Carabineiro SA, Bellabarba RM, Gomes PT, Pascu SI, Veiros LF, Freire C, et al. Inorg Chem 2008;47:8896–911.

h) Gomes CSB, Suresh D, Gomes PT, Veiros LF, Duarte MT, Nunes TG, et al. Dalton Trans 2010;39:736–48.

i) Gomes CSB, Carabineiro SA, Gomes PT, Duarte MT. Inorg Chim Acta 2011;367:151-7.

j) Gomes CSB, Duarte MT, Gomes PT. J Organomet Chem 2014;760:167–76.

k) Li L-D, Gomes CSB, Gomes PT, Duarte MT, Fan Z, Dalton Trans. 2011;40:3365–80.

l) Mashima K, Tsuguri H. J Organomet Chem 2005;690:4414–23 and references cited therein.

[4] Holm RH, Chakravorty A, Theriot L. J Inorg Chem 1966;5:625–35 and references cited therein.

[5] Yang L-Y, Chen Q-Q, Yang G-Q, Ma J-S. Tetrahedron 2003;59:10037–41.

[6] Crestani MG, Manbeck GF, Brennessel WW, McCormick TM, Eisenberg R. Inorg Chem 2011;50:7172–88.

[7] Gomes CSB, Gomes PT, Di Paolo RE, Macanita AL, Duarte MT, Calhorda MJ. Inorg Chem 2009;48:11176–86.

[8] a) Suresh D, Gomes CSB, Gomes PT, Di Paolo RE, Maçanita AL, Calhorda MJ, et al. Dalton Trans 2012;41:8502-05; Errata: Dalton Trans 2012;41: 14713 and Dalton Trans 2013;42:16969.

b) Calhorda MJ, Suresh D, Gomes PT, Di Paolo RE, Maçanita AL. Dalton Trans 2012;41:13210–7.

c) Suresh D, Lopes PS, Ferreira B, Figueira CA, Gomes CSB, Gomes PT, et al. Chem Eur J 2014;20:4126–40.

[9] Suresh D, Gomes CSB, Lopes PS, Figueira CA, Ferreira B, Gomes PT, et al. Chem Eur J 2015;21:9133–49.

[10] Suresh D, Ferreira B, Lopes PS, Krishnamoorthy P, Gomes CSB, Charas A, et al. Dalton Trans. 2016;45:15603–20.

[11] a) Grushin VV, Marshall WJ. Adv Synth Catal 2004;346:1457–60.

b) Matsui S, Yoshida Y, Takagi Y, Spaniol TP, Okuda J. J Organomet Chem 2004;689:1155–64.

c) Yoshida Y, Matsui S, Takagi Y, Mitani M, Nakano T, Tanaka H, et al. Organometallics 2001;20:4793–9.

[12] a) Lash TD, Chandrasekar P, Osuma AT, Chaney ST, Spence JD. J Org Chem 1998, 63, 8455–69.

b) Novak BH, Lash TD. J Org Chem 1998;63:3998–4010.

c) Lash TD, Bellettini JR, Bastian JA, Couch KB. Synthesis 1994;170–2.

[13] Parr RG, Yang W. Density Functional Theory of Atoms and Molecules. New York: Oxford University Press; 1989.

[14] a) te Velde G, Bickelhaupt FM, van Gisbergen SJA, Guerra CF, Baerends EJ, Snijders JG, et al. J Comp Chem 2001;22:931–67.

b) Guerra CF, Snijders JG, te Velde G, Baerends EJ. Theor Chem Acc 1998;99:391–403.

c) ADF2013. SCM. Theoretical Chemistry. Vrije Universiteit, Amsterdam, The Netherlands, http://www.scm.com.

[15] a) van Gisbergen SJA, Groeneveld JA, Rosa A, Snijders JG, Baerends EJ. J Phys Chem A 1999;103:6835-44.

b) Rosa A, Baerends EJ, van Gisbergen SJA, van Lenthe E, Groeneveld JA, Snijders JG, J Am Chem Soc 1999;121:10356-65.

c) van Gisbergen SJA, Rosa A, Ricciardi G, Baerends EJ. J Chem Phys 1999;111:2499-506.

d) van Gisbergen SJA, Snijders JG, Baerends EJ. Comp Phys Comm 1999;118:119-38.

e) Moussa J, Chamoreau L-M, Esposti AD, Gullo MP, Barbieri A, Amouri H. Inorg Chem 2014;53:6624-33.

[16] Wang F, Ziegler T. J Chem Phys 2005;123:154102– 13.

[17] Burla MC, Caliandro R, Camalli M, Carrozzini B, Cascarano GL, De Caro L, et al. J Appl Crystallogr 2005;38:381–8.

[18] Burla MC, Caliandro R, Carrozzini B, Cascarano GL, Cuocci C, Giacovazzo C, et al. J Appl Crystallogr 2015;48, 306-9.

[19] Sheldrick GM. Acta Cryst 2008;A64:112-22.

[20] Farrugia LJ. J Appl Cryst 1999;32:837-8.

[21] Macrae F, Bruno IJ, Chisholm JA, Edgington PR, McCabe P, Pidcock E, et al. J Appl Cryst 2008;41:466-70.

[22] Spek AL. J Appl Crystallogr 2003;36:7–13.

[23] Ferreira B, Silva PF, Seixas de Melo JS, Pina J, Maçanita AL. J Phys Chem B 2012;116:2347-55.

[24] Stricker G. In Effective Implementation of Modulation Functions in Deconvolution and Reconvolution of Analytical Signals. Bouchy M, editor. Nancy, France: University Press; 1982.

[25] Vosko SH, Wilk L, Nusair M. Can J Phys 1980:58:1200–11.

[26] Becke AD. J Chem Phys 1987;88:1053–62.

[27] a) Perdew JP. Phys Rev B 1986;33:8822–4.

b) Perdew JP. Phys Rev B 1986;34:7406.

[28] van Lenthe E, Ehlers A, Baerends EJ. J Chem Phys 1999;110:8943–53.

[29] (a) Perdew JP, Burke K, Ernzerhof M. Phys Rev Lett 1996;77:3865–8.

(b) Perdew JP, Burke K, Ernzerhof M. Phys Rev Lett 1997;78:1396.

[30] Portmann S, Lüthi HP. Chimia 2000;54:766–70.

[31] Chemcraft Program. http://www.chemcraftprog.com/index.html [last accessed 22.08.2016].

[32] Morgado J, Charas A, Fernandes JA, Gonçalves IS, Carlos LD, Alcácer L. J Phys D: Appl Phys 2006;39:3582–7.

- 2-(*N*-alkylimino)pyrrole ligand precursors and its boron complexes were synthesized
- Fluorescence properties of these blue/violet emitting compounds were studied
- Non-radiative decays are much weaker than those of the *N*-2,6-$R_2$-arylimino analogues
- DFT and TDDFT calculations support the experimental results
- Simple OLED devices reveal maximum luminances of *ca.* 90 cd $m^{-2}$